GASTROENTEROLOGY 2005;129:696–705

Autophagic Cell Death of Pancreatic Acinar Cells in Serine Protease Inhibitor Kazal Type 3–Deficient Mice

MASAKI OHMURAYA,*,† MASAHIKO HIROTA,† MASATAKE ARAKI,§ NOBORU MIZUSHIMA,‖,¶ MAKOTO MATSUI,‖,# TAKAO MIZUMOTO,†,** KYOKO HARUNA,* SHOEN KUME,†† MOTOHIRO TAKEYA,** MICHIO OGAWA,† KIMI ARAKI,* and KEN-ICHI YAMAMURA*

*Division of Developmental Genetics, Institute of Molecular Embryology and Genetics, Kumamoto University, Kumamoto; †Departments of Surgery, Faculty of Medical and Pharmaceutical Sciences, Kumamoto University, Kumamoto; §Division of Bioinformatics, Institute for Resource Development and Analysis, Kumamoto University, Kumamoto; ‖Department of Bioregulation and Metabolism, Tokyo Metropolitan Institute of Medical Science, Tokyo; ¶Time's Arrow and Biosignaling, PRESTO, Japan Science and Technology Agency, Kawaguchi; #Department of Molecular Biomechanics, School of Life Science, The Graduate University for Advanced Studies, Okazaki; **Division of Cell Pathology, Faculty of Medical and Pharmaceutical Sciences, Kumamoto University, Kumamoto; and ††Division of Stem Cell Biology, Institute of Molecular Embryology and Genetics, Kumamoto University, Kumamoto, Japan

Background & Aims: Serine protease inhibitor Kazal type 1 (SPINK1), which is structurally similar to epidermal growth factor, is thought to inhibit trypsin activity and to prevent pancreatitis. Point mutations in the *SPINK1* gene seem to predispose humans to pancreatitis; however, the clinical significance of *SPINK1* mutations remains controversial. This study aimed to elucidate the role of SPINK1. *Methods:* We generated *Spink3*-deficient (*Spink3*$^{-/-}$) mice by gene targeting in mouse embryonic stem cells. Embryonic and neonatal pancreases were analyzed morphologically and molecularly. Specific probes were used to show the typical autophagy that occurs during acinar cell death. *Results:* In *Spink3*$^{-/-}$ mice, the pancreas developed normally up to 15.5 days after coitus. However, autophagic degeneration of acinar cells, but not ductal or islet cells, started from day 16.5 after coitus. Rapid onset of cell death occurred in the pancreas and duodenum within a few days after birth and resulted in death by 14.5 days after birth. There was limited inflammatory cell infiltration and no sign of apoptosis. At 7.5 days after birth, residual ductlike cells in the tubular complexes strongly expressed pancreatic duodenal homeodomain-containing protein 1, a marker of pancreatic stem cells, without any sign of acinar cell regeneration. *Conclusions:* The progressive disappearance of acinar cells in *Spink3*$^{-/-}$ mice was due to autophagic cell death and impaired regeneration. Thus, Spink3 has essential roles in the maintenance of integrity and regeneration of acinar cells.

Inappropriate activation of trypsinogen in the pancreas leads to pancreatitis. Once activated, trypsin is capable of activating many other digestive proenzymes in the pancreas and enhances autodigestion of the pancreas. Trypsin activity is thought to be predominantly controlled by the serine protease inhibitor Kazal type 1 (SPINK1), which is also known as pancreatic secretory trypsin inhibitor. In the mouse, this homologous gene is designated as *Spink3* (serine protease inhibitor Kazal type 3). SPINK1 is synthesized in the acinar cells of the pancreas and binds to trypsin to prevent further activation of pancreatic enzymes when trypsinogen is converted into trypsin. Thus, a lack of SPINK1 may result in the premature conversion of trypsinogen into active trypsin in acinar cells, thus leading to autodigestion of the exocrine pancreas by activated proteases. It is interesting to note that SPINK1 and epidermal growth factor (EGF) have structural similarities, including the number of amino acid residues and the presence of 3 intrachain disulfide bridges.[1] SPINK1 has been found to induce the proliferation of a variety of cell lines.[2,3]

Several mutations of the trypsinogen gene have been identified and are assumed to be pathogenic in patients with hereditary pancreatitis through the enhancement of intrapancreatic trypsin activity.[4,5] Although the mutations lead to an 80% likelihood of developing pancreatitis, they are not found in approximately 50% of patients. Mutations in the cystic fibrosis transmembrane conductance regulator are found in patients with chronic and idiopathic pancreatitis.[6,7] However, additional gene mutations remain to be identified. Although the association of several mutations in the *SPINK1* gene with familial

Abbreviations used in this paper: EGF, epidermal growth factor; ES, embryonic stem; GFP, green fluorescent protein; LC3, microtubule-associated protein 1 light chain 3; PCR, polymerase chain reaction; Pdx1, pancreatic duodenal homeodomain-containing protein 1; RT-PCR, reverse-transcription polymerase chain reaction; SPINK1, serine protease inhibitor Kazal type 1; TUNEL, terminal deoxynucleotidyl transferase–mediated deoxyuridine triphosphate nick-end labeling.

0016-5085/05/$30.00
doi:10.1053/j.gastro.2005.05.057

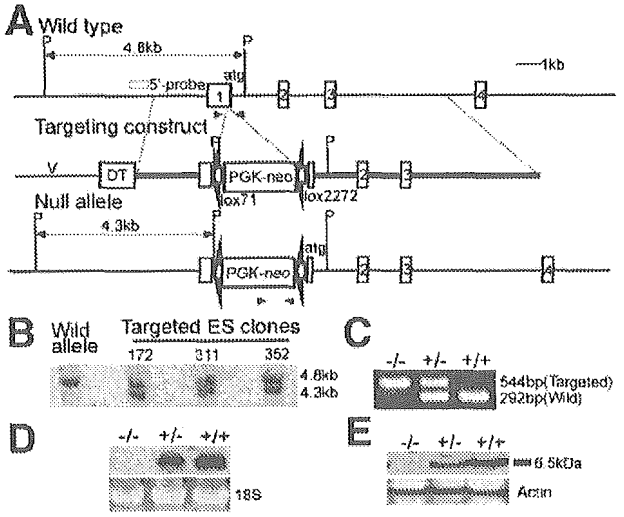

Figure 1. Targeted inactivation of the *Spink3* gene and genotype analysis. (*A*) Schematic maps of the wild-type *Spink3* locus and 5′ probe (*top*), the targeting vector (*middle*), and the mutated allele (*bottom*). Exons and 5′ probes are shown as *open boxes*. Mouse genomic and bacterial (V) sequences are shown by *heavy* and *thin lines*, respectively. Diphtheria toxin A fragment (DT) and neo, shown as *open boxes*, are in the same transcriptional orientation to the *Spink3* gene. Cleavage at *Pst*I sites (P) was used to distinguish between wild-type and mutant alleles. *Closed triangles* are PCR primers. (*B*) Southern blot analysis of *Pst*I-digested genomic DNA of ES cells with the 5′ probe, as shown in (*A*). (*C*) PCR analysis for genotyping. The PCR pair flanking the neo cassette detected a 292–base pair band in the wild type and hetero type, but not in the homozygote. (*D*) Northern blot analysis. (*E*) Western blot analysis. PGK, phosphoglycerate kinase.

and juvenile pancreatitis has been reported,[8–11] the clinical significance of these mutations remains controversial.[12–17] To elucidate the role of *Spink3*, we produced *Spink3*-null mutant mice by gene targeting in mouse embryonic stem (ES) cells.

Materials and Methods

Gene-Targeting Construction and Generation of *Spink3*$^{-/-}$ Mice

Genomic DNA containing all the exons of the *Spink3* gene was isolated from a C57BL/6-EMBL3 library (a gift from Dr Aizawa, Riken, Kobe, Japan) by hybridization with an 800–base pair genomic DNA probe containing intron 1. The targeting construction was produced in pBluescript II (Stratagene, La Jolla, CA) containing the phosphoglycerate kinase 1 promoter and the neomycin resistance gene (neo) cassette flanked by the mutated *lox*P sites *lox*71 and *lox*2272[18] and the diphtheria toxin A fragment with a polyadenylation cassette by using a polyoma enhancer/herpes simplex virus thymidine kinase promoter. The neo cassette was inserted in front of the initiation codon (Figure 1*A*). Electroporation with TT2 ES cells[19] (a gift from Dr Aizawa) and colony isolation were performed as previously described.[20] Three targeted ES clones were obtained from among 360 G418-resistant clones. ES cells were aggregated with ICR molura as described.[20] Chimeras were mated with C57BL/6J mice, and germline transmission was obtained for all 3 lines. Noon on the day of vaginal plug detection was defined as 0.5 days after coitus. All experiments were performed in accordance with the Declaration of Helsinki and were approved by the Kumamoto University Ethics Committee for Animal Experiments.

Cerulein-Induced Pancreatitis

After overnight fasting, *Spink3*$^{+/+}$ and *Spink3*$^{+/-}$ mice (5–7 weeks old and weighing 18–23 g) were given hourly intraperitoneal injections of saline as control (n = 5) or saline containing a supramaximal stimulating concentration of cerulein (50 μg/kg; n = 5) (Sigma-Aldrich Corp, Tokyo, Japan) for several hours (3–12 hours). One hour after the last injection, mice were killed, and the serum and pancreas were rapidly prepared for study. The serum was used for measurement of amylase activity. The pancreas was used for Western blot and trypsin assay analysis.

DNA and RNA Analysis

DNA was digested with *Pst*I and subjected to Southern blot hybridization. For genotyping of embryos and pups, polymerase chain reaction (PCR) analysis was performed with the following primers: neo cassette, 5′-AGAGGCTATTCGGCTATGAC-3′ and 5′-CACCATGATATTCGGCAAGC-3′; *Spink3* exon 1, 5′-AGTTCTTCTGGCTTTTGCACCC-3′; and *Spink3* intron 1, 5′-CTTTGCCACCACATCCCAAATG-3′. Total RNA was isolated from the trunk or intestine with Sepasol (Nacalai Tesque, Kyoto, Japan). For Northern blot analysis, 10 μg of RNA was applied to each lane and fractionated on a 1.4% agarose gel. Filter-bound RNA was sequentially hybridized with a digoxigenin-labeled RNA probe (Roche Molecular Biochemicals, Mannheim, Germany). Reverse-transcription PCR (RT-PCR) analysis was performed with the following primers: *Spink3*, 5′-AGTTCTTCTGGCTTTTGCACCC-3′ and 5′-CTCTTTTCCAGTCACCTTAGCT-3′; and trypsinogen, 5′-TGGCTTCCTAGAGGGAGGCAA-3′ and 5′-CACAGCCATAGCCCCAAGAGAC-3′.

Western Blot Analysis

The pancreas was homogenized in lysate buffer (HEPES 50 mmol/L, pH 7.4, NaCl 150 mmol/L, Triton X-100 0.1%, glycerol 10%, NaF 1 mmol/L, sodium orthovanadate 2 mmol/L, ethylenediaminetetraacetic acid 1 mmol/L, and protease inhibitor cocktail [1:100 dilution; Sigma-Aldrich]). Extracts (20 μg of protein per lane) were applied to 20% (for *Spink3* detection) or 16% (for microtubule-associated protein 1 light chain 3 [LC3] detection) polyacrylamide gel electrophoresis and transferred to an Immobilon polyvinylidene difluoride filter (Millipore, Billerica, MA). Primary antibodies to the following antigens (made in rabbit) were used at the indicated dilutions: pancreatic secretory trypsin inhibitor (Transgenic Inc, Kumamoto, Japan), 1:500; and LC3 (provided by Dr Tamotsu Yoshimori), 1:2000. An anti-rabbit

immunoglobulin G antibody conjugated with horseradish peroxidase (Amersham Biosciences Corp, Piscataway, NJ) was used for detection. Quantification of the ratio of LC3-II to LC3-I was performed by the Densitograph software library version 4 (Atto, Tokyo, Japan). Unpaired Student *t* tests were used to calculate *P* values.

Histological and Immunohistochemical Analysis

For histological analysis, tissue was fixed overnight in 10% formalin, embedded in paraffin, sectioned, and stained with the H&E procedure. Immunohistochemistry was performed by using the following primary antibodies: rabbit anti-insulin antibody (diluted 1:200; Santa Cruz Biotechnology, Inc, Santa Cruz, CA); rabbit anti-glucagon antibody (Dako, Carpinteria, CA); goat anti-amylase antibody (diluted 1:200; Santa Cruz); rabbit anti-pancreatic duodenal homeodomain-containing protein 1 (Pdx1) antibody (diluted 1:500; Chemicon International, Inc, Temecula, CA); and monoclonal anti–proliferating cell nuclear antigen antibody (diluted 1:500; Novocastra Laboratories Ltd, Newcastle upon Tyne, UK). Reactivity of the primary antibodies with mouse antigens was confirmed. Primary antibodies were detected with a commercial biotin-streptavidin system (Vector Laboratories, Burlingame, CA).

Bromodeoxyuridine Incorporation Analysis

To evaluate the type of cells that synthesize DNA in the pancreas, mice were given a single intraperitoneal dose (100 mg/kg body weight) of bromodeoxyuridine (Sigma-Aldrich), a thymidine analogue, and killed 24 hours later. Sections of the pancreas were processed for paraffin embedding and immunostaining with an anti-bromodeoxyuridine antibody (diluted 1:20; Dako).

Terminal Deoxynucleotidyl Transferase–Mediated Deoxyuridine Triphosphate Nick-End Labeling Assay

For the detection of apoptosis, terminal deoxynucleotidyl transferase–mediated deoxyuridine triphosphate nick-end labeling (TUNEL) assay was performed by using an in situ apoptosis detection kit (Wako, Osaka, Japan).

Electron Microscopy

Pancreatic tissues were fixed with 2.5% glutaraldehyde and postfixed with 1% osmium tetroxide. After dehydration in a graded series of ethanol and propylene oxide, the samples were embedded in epoxy resin. Ultrathin sections were stained with uranyl acetate and lead citrate and then imaged with an H-7500 electron microscope (Hitachi, Tokyo, Japan).

Generation of *Spink3*$^{-/-}$-Green Fluorescent Protein-LC3 Mice and Fluorescence Microscopy

Pancreases from *Spink3*$^{-/-}$-green fluorescent protein (GFP)-LC3 mice at 0.5 days after birth were dissected, fixed, and sectioned. GFP fluorescence was observed by using an IX81 fluorescence microscope (Olympus, Tokyo, Japan) equipped with an ORCA ER charge-coupled device camera (Hamamatsu Photonics, Hamamatsu, Japan).

Trypsin Assay

Trypsin activity of the pancreas was measured fluorometrically by using benzoyl-L-arginine *p*-nitroanilide as substrate according to previously described methods.[21] The trypsin activity was corrected to the density of pancreas DNA. Unpaired Student *t* tests were used to calculate *P* values. $P < .05$ was considered to indicate a significant difference.

Determination of Blood Glucose

Glucose was determined in the peripheral blood of *Spink3*$^{+/+}$, *Spink3*$^{+/-}$, or *Spink3*$^{-/-}$ mice at 0.5, 1.5, and 3.5 days after birth by use of commercial equipment (Glucocard) according to the supplier's instructions (Arkray, Inc, Kyoto, Japan).

Results

Generation of *Spink3*$^{-/-}$ Mice

The vector used for homologous recombination in ES cells to disrupt the *Spink3* locus is shown in Figure 1*A*. Three targeted ES clones lacking *Spink3* were identified by Southern blot analysis with a 5′ probe (Figure 1*B*) and were used to generate chimeric mice. *Spink3*$^{+/-}$ mice were healthy, fertile, and indistinguishable from their *Spink3*$^{+/+}$ littermates, although the level of Spink3 expression was approximately half that of their *Spink3*$^{+/+}$ littermates (Figure 1*D* and *E*). Male and female *Spink3*$^{+/-}$ mice were mated to produce *Spink3*$^{-/-}$ mice. Genotypes were determined by PCR analysis (Figure 1*C*). The ratio of living *Spink3*$^{+/+}$, *Spink3*$^{+/-}$, and *Spink3*$^{-/-}$ mice at 0.5 days after birth was 33:72:36 (n = 141), respectively. This matches the mendelian rate of 1:2:1. Thus, a *Spink3* deficiency does not cause embryonic lethality. In homozygous newborn mice, no Spink3 messenger RNA (mRNA) or protein was detected (Figure 1*D* and *E*), thus indicating the production of a null allele of the *Spink3* locus. At birth, *Spink3*$^{-/-}$ mice were indistinguishable macroscopically from their *Spink3*$^{+/+}$ and *Spink3*$^{+/-}$ littermates and were fed milk. However, *Spink3*$^{-/-}$ mice did not gain weight (Figure 2*A* and *B*) and died by 14.5 days after birth (Figure 2*C*). They were severely dehydrated and had thin, cracking skin with very little fur. *Spink3*$^{-/-}$ mice at 18.5 days after coitus had a normal liver, gallbladder, spleen, stomach, duodenum, bile duct, and other viscera. Similarly, the pancreas appeared almost normal at 18.5 days after coitus (Figure 2*D*), thus suggesting normal embryonic development of the pancreas. However, the pancreas progressively disap-

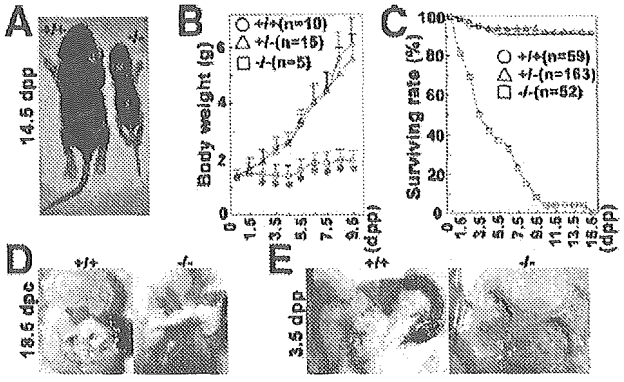

Figure 2. Analysis of *Spink3*$^{-/-}$ mice. (*A*) *Spink3*$^{-/-}$ mice at 14.5 days after birth, with severe growth retardation. (*B*) Growth curve of *Spink3*$^{+/+}$ (○), *Spink3*$^{+/-}$ (△), and *Spink3*$^{-/-}$ mice (□). (*C*) Survival rate of *Spink3*$^{+/+}$ (○), *Spink3*$^{+/-}$ (△), and *Spink3*$^{-/-}$ mice (□). (*D*) At 18.5 days after coitus, *Spink3*$^{-/-}$ mice had pancreatic tissue indistinguishable from that of their *Spink3*$^{+/+}$ littermates. (*E*) At 3.5 days after birth, *Spink3*$^{-/-}$ mice showed a transparent pancreatic bed and atrophic change in the spleen and are clearly distinguishable from their *Spink3*$^{+/+}$ littermates. $*P < .05$ (unpaired Student *t* test) vs *Spink3*$^{+/+}$ mice. dpp, days after birth; dpc, days after coitus.

peared after birth, and the duodenum became extended. The pancreatic bed was quite small and transparent, and the spleen was much smaller than that of wild-type mice at 3.5 days after birth (Figure 2*E*).

Reverse-Transcription Polymerase Chain Reaction Analysis

To examine when the *Spink3* and trypsinogen genes start to express, RT-PCR analyses were performed. *Spink3* mRNAs and trypsinogen mRNAs were detected in embryos at 11.5 and at 15.5 days after coitus, respectively.

Histological and Immunohistochemical Analysis of Pancreas and Gastrointestinal Tract

Histological and immunohistochemical studies were performed to analyze the cause of the pancreatic deficiency. At 15.5 days after coitus, pancreases were normal, with finely branched ducts and distinct lumen in both *Spink3*$^{+/+}$ and *Spink3*$^{-/-}$ embryos. At 16.5 days after coitus, acinar cells were clearly recognized in both *Spink3*$^{+/+}$ and *Spink3*$^{-/-}$ embryos (Figure 3*A*), but *Spink3*$^{-/-}$ embryos showed mild vacuolization of acinar cells (Figure 3*A*). This suggests that vacuolization begins at around the time when zymogen granules appear.

At 18.5 days after coitus, vacuolization of acinar cells became severe in *Spink3*$^{-/-}$ embryos (Figure 3*B*). At 0.5 days after birth, acinar cell degeneration was clearly evident in *Spink3*$^{-/-}$ mice (Figure 3*C*). At 1.5 days after birth, pancreatic lobules mainly comprised tubular complexes lined by flattened ductlike cells in a loose connective tissue stroma with few remaining acinar cells (Figure 3*D*). At 3.5 days after birth, degenerative changes became severe (Figure 3*E*), and only a few acinar cells were positive for amylase (Figure 3*J*). Until 3.5 days after birth, islets remained quite normal histologically, and the staining intensities for insulin (Figure 3*A–E*) and glucagon (data not shown) in *Spink3*$^{-/-}$ mice were similar to those in *Spink3*$^{+/+}$ embryos. At 7.5 days after birth, rapid loss of acinar cells resulted in lobular contraction and led to tightly clustered tubular complexes associated with small numbers of residual acinar cells (Figure 3*F*). It is interesting to note that inflammatory cell infiltration was scarce in the pancreases of *Spink3*$^{-/-}$ mice. Vacuolization or degeneration of acinar cells was not observed in either *Spink3*$^{+/+}$ or *Spink3*$^{+/-}$ mice at any stage (Figure 3*A–F*). These findings suggest that a lack of Spink3 activity induces massive selective acinar cell degeneration.

In *Spink3*$^{-/-}$ mice at 7.5 days after birth, the ductlike cells in tubular complexes strongly expressed Pdx1 antigen, a marker of pancreatic stem cells (Figure 3*L*). However, they showed no mitotic figures in H&E staining (Figure 3*F*), no positive immunostaining with proliferating cell nuclear antigen (Figure 3*L*), and no bromodeoxyuridine incorporation (data not shown). Thus, there is no evidence of regeneration of acini in *Spink3*$^{-/-}$ mice during the period of our observations. Although spleens were small, histological sections showed a normal structure. The duodenum and small intestine of *Spink3*$^{-/-}$ mice looked normal up to 1.5 days after birth. However, at 3.5 days after birth, it was expanded, with the thin smooth muscle layer and villi mostly degenerated (Figure 4); the degeneration was probably caused by the *Spink3* deficiency. In any case, atrophy of the pancreas by deficient exocrine function and degeneration of the duodenum and small intestine were likely to be the main causes of the severe retardation of growth and death of *Spink3*$^{-/-}$ mice. This is consistent with the data that mice lacking the gene encoding basic helix-loop-helix protein p48 died soon after birth because of a complete absence of exocrine pancreatic tissue.[22] Apoptosis did not seem to be involved in this process, because there was no increase in the number of apoptotic cells detected by TUNEL assay (data not shown).

Electron Microscopic Analysis of Pancreas

We also performed transmission electron microscopic analysis of the pancreas. At 18.5 days after coitus, the cytoplasm of acinar cells in *Spink3*$^{+/+}$ mice was filled with zymogen granules, but many vacuoles were observed in *Spink3*$^{-/-}$ mice (Figure 5*A*). At 0.5 days after

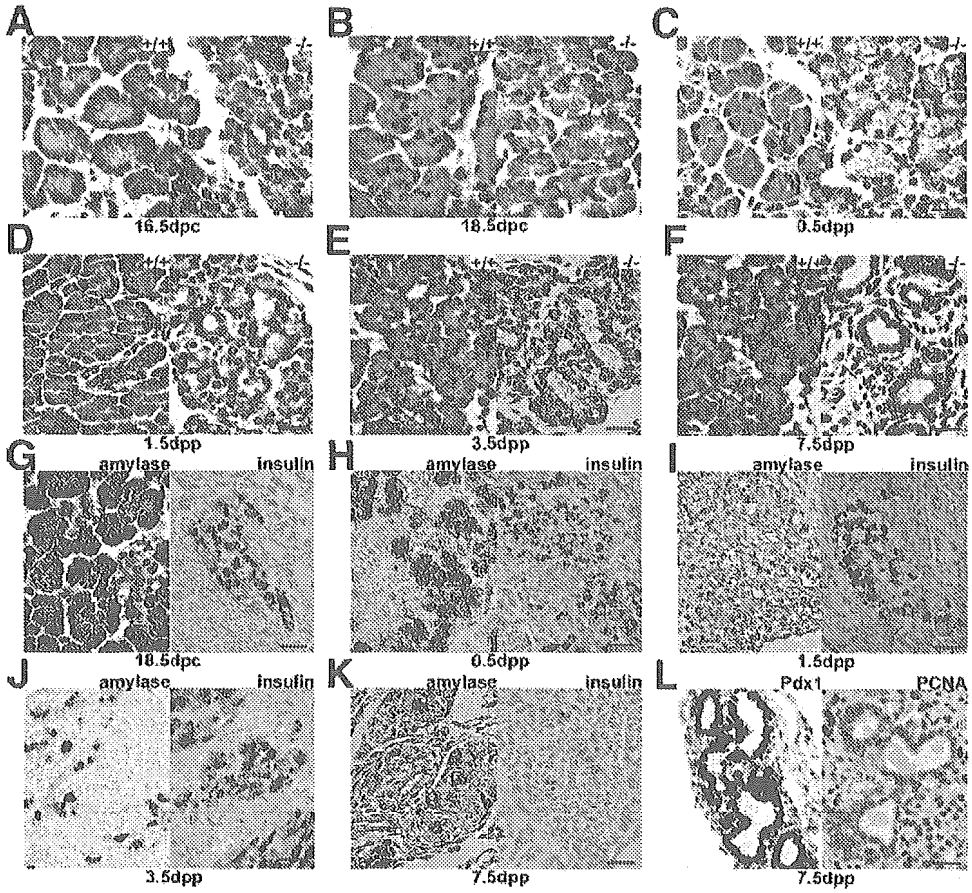

Figure 3. Histological and immunohistochemical analysis of the pancreas. At 16.5 days after coitus, pancreatic acinar cells are clearly visible in *Spink3*$^{+/+}$ and *Spink3*$^{-/-}$ (*A*), although the pancreases of *Spink3*$^{-/-}$ mice began to show mild vacuolization in the acinar cells. At 18.5 days after coitus and 0.5 days after birth, marked acinar cell vacuolization was observed in *Spink3*$^{-/-}$, but not in *Spink3*$^{+/+}$ (*B*). That pancreatic lobules mainly comprise the tubular complex lined by flattened ductlike cells in a loose connective tissue stroma with few remaining acinar cells was evident at 0.5 days after birth (*C*), and the loss of acinar cells became severe thereafter (*D–F*) in the pancreases of *Spink3*$^{-/-}$ mice. There were no abnormalities in *Spink3*$^{+/+}$ and *Spink3*$^{+/-}$ (*A–F*). The pancreas of a *Spink3*$^{-/-}$ mouse was stained for amylase up to 3.5 days after birth (*G–J*), but most acinar cells positive for amylase disappeared rapidly, whereas the endocrine cells retained their morphology and function (*J* and *K*). The pancreas at 7.5 days after birth of a *Spink3*$^{-/-}$ mouse was stained for Pdx1, but not for proliferating cell nuclear antigen (*L*) (bars = 20 μm). dpp, days after birth; dpc, days after coitus.

birth, *Spink3*$^{-/-}$ acinar cells showed extensive vacuolization, but only a small amount of vacuolization was observed in *Spink3*$^{+/+}$ mice (Figure 5*B*). At a higher magnification, some vacuoles were found to contain cellular organelles, thus indicating that they were autophagic vacuoles (Figure 5*C*). Nuclear changes and apoptotic body formation were not observed (Figure 5*D*). Endocrine (arrowhead in Figure 5*E*) and ductal epithelial (arrow in Figure 5*E* and *F*) cells showed normal structures. At 1.5 days after birth, both the number and size of acinar cells were markedly reduced in *Spink3*$^{-/-}$ mice (Figure 5*F*), and those remaining contained various types of vacuoles compressing the nuclei and resulting in cell death (Figure 5*G*). Occasionally, a huge vacuole containing various digested organelles was observed (Figure 5*H*). Some of the degenerated acinar cells were phagocytosed by macrophages (Figure 5*I*). These morphological findings showed that the massive amount of acinar cell death in *Spink3*$^{-/-}$ mice was associated neither with substantial infiltration of inflammatory cells, as found in necrosis, nor with apoptosis, the best characterized form of programmed cell death. The appearance of numerous cytoplasmic vacuoles before nuclear alteration indicates that acinar cell death in *Spink3*$^{-/-}$ mice is similar to an autophagic cell death, a form of major physiological cell death.[23–25]

Autophagic Degeneration in *Spink3*$^{-/-}$ Mice and Acute Pancreatitis

To confirm the presence of autophagosomes, we analyzed the expression of LC3, an autophagosome-associated protein.[26] There are 2 forms of LC3 protein: LC3-I

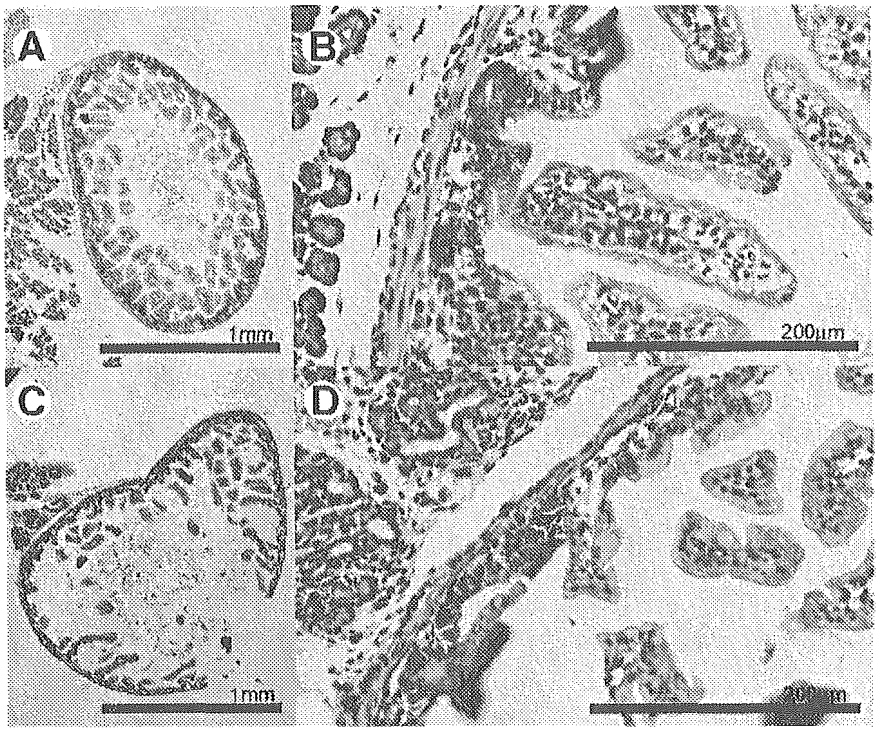

Figure 4. Histological analysis of the duodenum. (*A* and *B*) Duodenum of *Spink3*$^{+/+}$. (*C* and *D*) Duodenum of *Spink3*$^{-/-}$. At 3.5 days after coitus, the duodenum of *Spink3*$^{-/-}$ mice is expanded, with the thin smooth muscle layer and villi mostly degenerated.

and LC3-II. Cytosolic LC3-I protein (18 kilodaltons) is converted into LC3-II (16 kilodaltons) and is associated with the autophagosome membrane. The amount of LC3-II is thus correlated with the extent of autophagosome formation. As shown in Figure 6*A*, *Spink3*$^{-/-}$ pancreases possessed more LC3-II than those of *Spink3*$^{+/+}$, as in mice with cerulein-induced pancreatitis (Figure 6*C*). Densitometric analysis showed that the ratio of LC3-II to LC3-I was 0.56 (SD, 0.24) and 2.23 (SD, 0.10) in *Spink3*$^{+/+}$ and *Spink3*$^{-/-}$ mice, respectively. The ratio of LC3-II to LC3-I was 0.70 (SD, 0.46) and 2.06 (SD, 0.57) in control mice and mice with cerulein-induced pancreatitis, respectively. Thus, the amount of LC3-II increased in *Spink3*$^{-/-}$ mice, thus suggesting that autophagic activity is appreciably promoted in the *Spink3*$^{-/-}$ pancreas. Furthermore, we used GFP-LC3 mice, in which the expression and localization of LC3 can be monitored by the detection of GFP fluorescence.[27] In *Spink3*$^{+/-}$-GFP-LC3 mice at 0.5 days after birth, only a few dots of fluorescence were detected in the cytoplasm of acinar cells (Figure 6*B*, left). In contrast, many fluorescent dots were observed in the cytoplasm of acinar cells of *Spink3*$^{-/-}$-GFP-LC3 mice at 0.5 days after birth (Figure 6*B*, right). Some dots can be recognized as ringlike structures, which may represent the attachment of GFP-LC3 protein to the autophagosome membrane. The number of GFP-LC3 dots was fewer than that of vacuoles observed by electron microscopy. We believe that this difference can be explained by the fact that LC3 gradually dissociates from the autophagic vacuoles after fusion with lysosomes. These results suggest extensive autophagosome formation in *Spink3*$^{-/-}$ acinar cells. Serum amylases were increased in *Spink3*$^{-/-}$ mice at 0.5 days after coitus as in mice with cerulein-induced pancreatitis (Figure 6*D*). This suggests that the last moment of cell death is accompanied by disruption of the membrane, thus releasing various cellular constituents, including amylase.

Cerulein-Induced Pancreatitis

In *Spink3*$^{+/+}$ mice, the serum amylase level after 3, 6, and 9 injections was 14,080, 17,860, and 33,800 IU/L, respectively (n = 5). In *Spink3*$^{+/-}$ mice, the serum amylase level after 3, 6, and 9 injections was 12,000, 20,500, and 33,620 IU/L, respectively (n = 5). These results suggest that there is no difference in sensitivity to cerulein-induced pancreatitis. In addition, there was no significant difference in trypsin activities after 9 injections in *Spink3*$^{+/+}$ mice (0.25 unit [Optical Density (OD)/DNA concentration (μg/μL)] SD = 0.03; n = 5) or *Spink3*$^{+/-}$ mice (0.23 SD = 0.02; n = 5), although

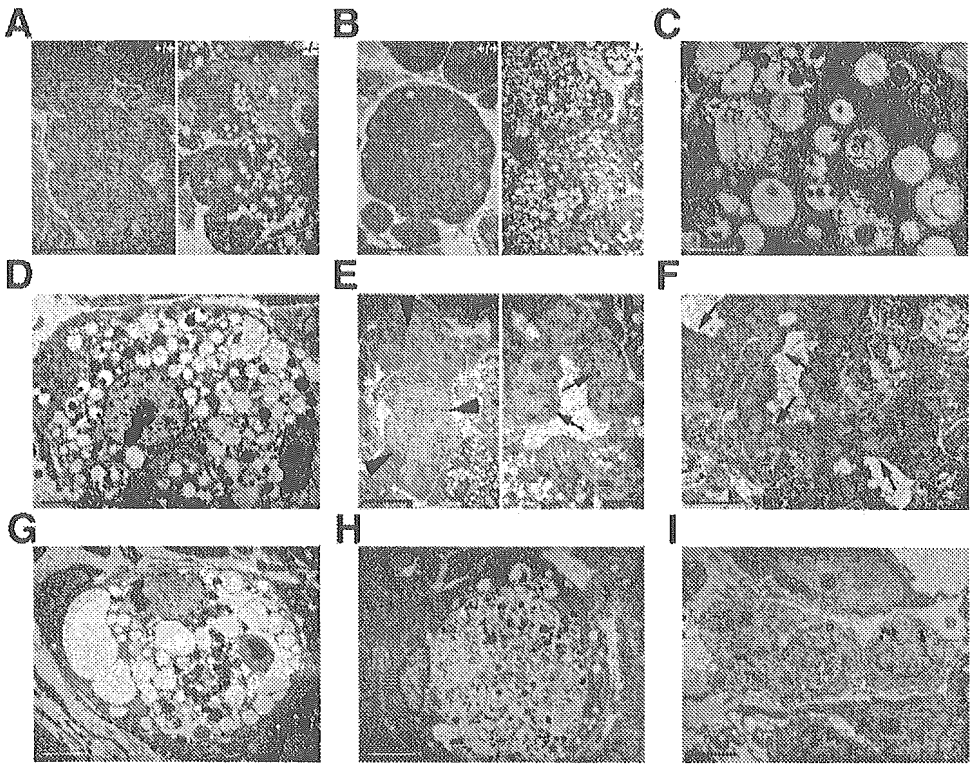

Figure 5. Electron microscopy. (*A*) Zymogen granules in *Spink3*$^{+/+}$ acinar cells and vacuolization in *Spink3*$^{-/-}$ acinar cells at 18.5 days after coitus. (*B*) Significant acinar cell vacuolization in the *Spink3*$^{-/-}$ pancreas, but not in *Spink3*$^{+/+}$, at 0.5 days after birth. (*C*) Vacuoles containing degenerated organelles. (*D*) The intact nucleus. (*E*) Normal islet and ductal epithelial cells. (*F*) Abnormal and remaining acinar cells with various types of vacuoles in *Spink3*$^{-/-}$ mice at 1.5 days after birth. Nucleus degradation (*G*) and acinar cell death (*H*). (*I*) Phagocytosis of degenerated acinar cells by infiltrating macrophages. *Bars* = 12 μm (*A*, *B*, and *F*), 1.5 μm (*C*), 4 μm (*D*), 19 μm (*E*), 2.2 μm (*G*), 3.5 μm (*H*), and 3 μm (*I*).

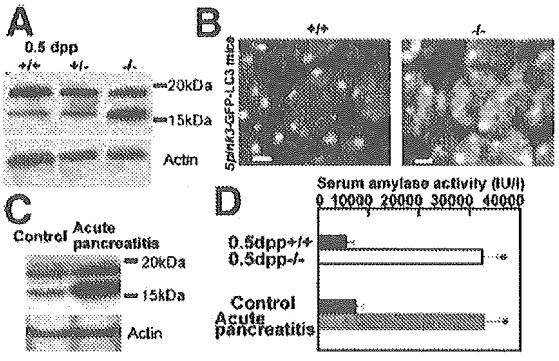

Figure 6. Analysis of LC3 expression in *Spink3*$^{-/-}$ and acute pancreatitis mice. (*A*) Western blot analysis of LC3 proteins extracted from the pancreas of *Spink3*$^{+/+}$, *Spink3*$^{+/-}$, and *Spink3*$^{-/-}$ at 0.5 days after birth. The upper band (18 kilodaltons) is LC3-I, and the lower band (16 kilodaltons) is LC3-II. (*B*) Fluorescence distribution in acinar cells of *Spink3*$^{+/-}$-GFP-LC3 and *Spink3*$^{-/-}$-GFP-LC3 mice at 0.5 days after birth (*bars* = 10 μm). (*C*) Western blot analysis of pancreatic LC3 expression in adult *Spink3*$^{+/+}$ mice with acute pancreatitis. (*D*) Serum amylase levels in *Spink3*$^{+/+}$ (*closed bar*; n = 5) and *Spink3*$^{-/-}$ mice (*open bar*; n = 5) at 0.5 days after birth and in adult mice with acute pancreatitis: 12 cerulein injections (*gray bar*; n = 5) vs control (*closed bar*; n = 5). *$P < .05$ (unpaired Student *t* test) vs *Spink3*$^{+/+}$ mice or control mice of the same age. dpp, days after birth.

these activities were increased compared with those in mice with saline injection (0.19 SD = 0.03; n = 5).

Analysis of Trypsin Activity in the Pancreas

The trypsin activity in the pancreases of *Spink3*$^{-/-}$ mice (0.55 and 1.1 at 0.5 and 1.5 days after birth, respectively; n = 3) was almost equal to that in wild-type mice (0.68 and 1.02; n = 3) and hetero-type mice (0.59 and 0.94; n = 3), thus suggesting that trypsin is not significantly activated in *Spink3*$^{-/-}$ mice.

Determination of Blood Glucose

There were no significant differences in blood glucose levels of *Spink3*$^{+/+}$, *Spink3*$^{+/-}$, or *Spink3*$^{-/-}$ mice.

Discussion

We think that initially SPINK1 binds to trypsin to prevent activation of pancreatic enzymes and that a lack of SPINK1 may result in the premature conversion of trypsinogen into active trypsin within acinar cells, thus leading to autodigestion of the exocrine pancreas by activated proteases. However, in *Spink3*$^{-/-}$ mice, auto-

phagic degeneration of acinar cells appeared at 16.5 days after coitus, and the rapid onset of cell death occurred in the pancreas and duodenum within a few days after birth, thus resulting in death by 14.5 days after birth. Thus, *Spink3* has essential roles for maintenance of the integrity and regeneration of acinar cells during the perinatal stage.

Spink3$^{-/-}$ mice died by 14.5 days after birth. Blood glucose levels were approximately the same in *Spink3*$^{+/+}$, *Spink3*$^{+/-}$, and *Spink3*$^{-/-}$ mice at 3.5 days after birth, when approximately 50% of *Spink3*$^{-/-}$ mice had already died. Thus, postnatal death may be due to exocrine dysfunction of the pancreas caused by the loss of acinar cells, but not of endocrine cells, and to malabsorption caused by degeneration of the duodenum. The loss of acinar cells can be caused by 1 of 3 mechanisms: necrosis, apoptosis, or autophagic cell death. When acute pancreatitis is induced by inappropriate activation of trypsinogen in the pancreas, necrosis is usually observed in the pancreas. Necrosis is characterized by the early swelling of both cells and organelles and by the loss of plasma membrane integrity. In *Spink3*$^{-/-}$ mice, swelling of acinar cells and organelles was not detected, and the plasma membrane was preserved without any scattering of the cellular contents. Apoptosis is a distinct form of programmed cell death, involves the orchestrated action of catabolic enzymes (proteases and nucleases) within the limits of intact plasma membranes, and is accompanied by a characteristic change in nuclear morphology, chromatin biochemistry, and stepwise DNA degradation. In *Spink3*$^{-/-}$ mice, apoptotic body formation was not observed, and TUNEL staining was negative. In contrast, acinar cell death observed in *Spink3*$^{-/-}$ mice was characterized by the appearance of vacuoles that were considered to be autophagosomes, as shown by the detection of more LC3-II than of LC3-I. A rapid increase of autophagosomes after birth may result in acinar cell death. These results suggest that the loss of acinar cells is caused by autophagic cell death and not by necrosis or apoptosis.

Autophagy is a dynamic process that involves several steps: the rearrangement of subcellular membranes to sequester the cytoplasm and organelles to form autophagosomes, the assembly of these autophagosomes with lysosomes, and the formation of autolysosomes, where the sequestered cargo is degraded and recycled.[28] Although the primary roles of this degenerative pathway are the normal turnover of cytoplasmic constituents and a response to starvation, it might also be important for the digestion and removal of abnormal proteins that would otherwise accumulate in cells. In addition to maintaining cellular homeostasis, there is growing evidence regarding the participation of autophagy in processes such as cellular differentiation, tissue remodeling, growth control, cell defense, and adaptation to adverse environments. In fact, mice deficient for Atg5, which is essential for autophagosome formation, die within 1 day of delivery but appear almost normal at birth.[29] Autophagic cell death is 1 type of programmed cell death. In contrast to apoptosis, cell death occurs independently of caspases,[30,31] and mitochondria are degraded, although a few are required for the supply of adenosine triphosphate while the cytoskeleton remains intact.

In this study, we have shown that autophagy typically occurs during acinar cell death in *Spink3*$^{-/-}$ mice. The most prominent feature of *Spink3*$^{-/-}$ mice is the appearance of autophagosomes in acinar cells. This can be caused by 2 ways; 1 is that autophagosomes seem to play a protective role in the degradation of activated pancreatic enzymes, which are cytotoxic to acinar cells. In *Spink3*$^{-/-}$ mice, the absence of Spink3 may result in the activation of trypsin within acinar cells and may lead to the activation of other pancreatic enzymes; this may trigger the appearance of autophagosomes to degrade activated digestive enzymes, including activated trypsin. If this were the case, we should observe evidence of trypsin activation, and the appearance of the autophagosome should coincide with the expression of trypsinogen in *Spink3*$^{-/-}$ mice. As described in Results, trypsin was not significantly activated in *Spink3*$^{-/-}$ mice.

Han et al[32] reported that the mRNA expression of trypsinogen genes in the rat starts as early as 12 days after coitus and that it increases during embryonic development. Other groups have reported that active trypsin in rat was detected only at the end of the fetal period.[33,34] Our RT-PCR analysis showed that trypsin mRNA can be detected at 15.5 days after coitus. However, we do not know what amount of trypsin is required for autophagosome formation. Thus, it is not clear whether the appearance of the autophagosome coincides with the expression of the trypsinogen gene. In any case, activation of trypsin may not be related to autophagosome formation. The second possibility is that Spink3 regulates the formation of autophagosomes in acinar cells and that a deficiency in Spink3 may lead to the formation of numerous autophagosomes, thus leading to autophagic cell death. Further analyses will be required to test this possibility. Currently, the reason for the increase of amylase is not known. However, it may be explained as follows. In *Spink3* knockout mice, autophagosome formation is rapid and massive in the pancreas, as shown by electron microscopic studies and LC3 Western blot analysis. Thus, all autophagosomes may not be fused with lysosomes to form autolysosomes, or the number of lysosomal enzymes may not be enough for complete deg-

radation of cellular constituents. Finally, acinar cell death may occur by constitutive activation of autophagy,[35] thus resulting in the release of intact cell constituents, including digestive enzymes.

In *Spink3*$^{-/-}$ mice, extensive autophagic cell death was not accompanied by the regeneration of acinar cells from the tubular complexes, even though these cells expressed Pdx1. Tubular complexes are usually found as an intermediate or end-stage lesion during acute and chronic pancreatitis, cystic fibrosis, and pancreatic cancer.[36] The massive degeneration of acinar cells induces the regeneration of acinar cells from tubular complexes. In experimental rat models for severe acute pancreatitis, marked mitotic activity and Pdx1 expression were observed in ductal cells and tubular complexes.[37] In contrast, Pdx1-positive cells were present in tubular complexes but did not show mitotic activity in *Spink3*$^{-/-}$ mice at 7.5 days after birth. SPINK1 has structural similarities to EGF, and mice that lack EGF receptors have been shown to have impaired branching morphogenesis due to a generalized proliferation defect of the pancreatic epithelia.[38] In addition, SPINK1 can stimulate the proliferation of a variety of cells,[2,3] and the *Spink3* gene is also expressed in extra-acinar cells, including pancreatic duct cells.[39] These findings suggest that Spink3 is a key growth and differentiation factor for the regeneration of acinar cells and that Spink3 is essential for maintaining exocrine integrity of the pancreas.

Recently, autophagy or autophagic cell death has been recognized as the major process in myopathies such as Danon disease[40] and in neurodegenerative diseases such as Parkinson disease,[41] Huntington disease,[42] and Alzheimer disease.[43] However, these findings have all been obtained from electron microscopic studies. The association of several mutations in the *SPINK1* gene with familial and juvenile pancreatitis has been reported[8–11]; given that this is the case, it is possible that pancreatitis is caused by autophagy, but not by the activation of trypsin. This fits with the notion that the SPINK1 mutation is more of a modifier for pancreatitis that potentiates the harmful effects of other genetic and environmental factors that actually initiate episodes of pancreatitis.

References

1. Yamamoto T, Nakamura Y, Nishide J, Emi M, Ogawa M, Mori T, Matsubara K. Molecular cloning and nucleotide sequence of human pancreatic secretory trypsin inhibitor (PSTI) cDNA. Biochem Biophys Res Commun 1985;132:605–612.
2. Ogawa M, Tsushima T, Ohba Y, Ogawa N, Tanaka S, Ishida M, Mori T. Stimulation of DNA synthesis in human fibroblasts by human pancreatic secretory trypsin inhibitor. Res Commun Chem Pathol Pharmacol 1985;50:155–158.
3. Nilnobu T, Ogawa M, Murata A, Nishijima J, Mori T. Identification and characterization of receptors specific for human pancreatic secretory trypsin inhibitor. J Exp Med 1990;172:1133–1142.
4. Whitcomb DC, Gorry MC, Preston RA, Furey W, Sossenheimer MJ, Ulrich CD, Martin SP, Gates LK Jr, Amann ST, Toskes PP, et al. Hereditary pancreatitis is caused by a mutation in the cationic trypsinogen gene. Nat Genet 1996;14:141–145.
5. Gorry MC, Gabbaizedeh D, Furey W, Gates LK Jr, Preston RA, Aston CE, Zhang Y, Ulrich C, Ehrlich GD, Whitcomb DC. Mutations in the cationic trypsinogen gene are associated with recurrent acute and chronic pancreatitis. Gastroenterology 1997;113: 1063–1068.
6. Sharer N, Schwarz M, Malone G, Howarth A, Painter J, Super M, Braganza J. Mutations of the cystic fibrosis gene in patients with chronic pancreatitis. N Engl J Med 1998;339:645–652.
7. Cohn JA, Friedman KJ, Noone PG, Knowles MR, Silverman LM, Jowell PS. Relation between mutations of the cystic fibrosis gene and idiopathic pancreatitis. N Engl J Med 1998;339:653–658.
8. Witt H, Luck W, Hennies HC, Classen M, Kage A, Lass U, Landt O, Becker M. Mutations in the gene encoding the serine protease inhibitor, Kazal type 1 are associated with chronic pancreatitis. Nat Genet 2000;25:213–216.
9. Pfutzer RH, Barmada MM, Brunskill AP, Finch R, Hart PS, Neoptolemos J, Furey WF, Whitcomb DC. SPINK1/PSTI polymorphisms act as disease modifiers in familial and idiopathic chronic pancreatitis. Gastroenterology 2000;119:615–623.
10. Chen JM, Mercier B, Audrezet MP, Raguenes O, Quere I, Ferec C. Mutations of the pancreatic secretory trypsin inhibitor (PSTI) gene in idiopathic chronic pancreatitis. Gastroenterology 2001;120: 1061–1064.
11. Kuwata K, Hirota M, Sugita H, Kai M, Hayashi N, Nakamura M, Matsuura T, Adachi N, Nishimori I, Ogawa M. Genetic mutations in exons 3 and 4 of the pancreatic secretory trypsin inhibitor in patients with pancreatitis. J Gastroenterol 2001;36:612–618.
12. Shimosegawa T. Do point mutations in the PSTI (SPINK1) gene truly contribute to the pathogenesis of chronic pancreatitis? J Gastroenterol 2001;36:645–647.
13. Whitcomb DC. How to think about SPINK and pancreatitis. Am J Gastroenterol 2002;97:1085–1088.
14. Threadgold J, Greenhalf W, Ellis I, Howes N, Lerch MM, Simon P, Jansen J, Charnley R, Laugier R, Frulloni L, et al. The N34S mutation of SPINK1 (PSTI) is associated with a familial pattern of idiopathic chronic pancreatitis but does not cause the disease. Gut 2002;50:675–681.
15. Chandak GR, Idris MM, Reddy DN, Bhaskar S, Sriram PV, Singh L. Mutations in the pancreatic secretory trypsin inhibitor gene (PSTI/SPINK1) rather than the cationic trypsinogen gene (PRSS1) are significantly associated with tropical calcific pancreatitis. J Med Genet 2002;39:347–351.
16. Drenth JP, te Morsche R, Jansen JB. Mutations in serine protease inhibitor Kazal type 1 are strongly associated with chronic pancreatitis. Gut 2002;50:687–692.
17. Kuwata K, Hirota M, Nishimori I, Otsuki M, Ogawa M. Mutational analysis of the pancreatic secretory trypsin inhibitor gene in familial and juvenile pancreatitis in Japan. J Gastroenterol 2003; 38:365–370.
18. Araki K, Araki M, Yamamura K. Site-directed integration of the cre gene mediated by Cre recombinase using a combination of mutant lox sites. Nucleic Acids Res 2002;30:e103.
19. Yagi T, Tokunaga T, Furuta Y, Nada S, Yoshida M, Tsukada T, Saga Y, Takeda N, Ikawa Y, Aizawa S. A novel ES cell line, TT2, with high germline-differentiating potency. Anal Biochem 1993; 214:70–76.
20. Araki K, Imaizumi T, Sekimoto T, Yoshinobu K, Yoshimuta J, Akizuki M, Miura K, Araki M, Yamamura K. Exchangeable gene trap using the Cre/mutated lox system. Cell Mol Biol (Noisy-le-Grand) 1999;45:737–750.

21. Kuwata K, Hirota M, Shimizu H, Nakae M, Nishihara S, Takimoto A, Mitsushima K, Kikuchi N, Endo K, Inoue M, et al. Functional analysis of recombinant pancreatic secretory trypsin inhibitor protein with amino-acid substitution. J Gastroenterol 2002;37: 928–934.
22. Krapp A, Knofler M, Ledermann B, Burki K, Berney C, Zoerkler N, Hagenbuchle O, Wellauer PK. The bHLH protein PTF1-p48 is essential for the formation of the exocrine and the correct spatial organization of the endocrine pancreas. Genes Dev 1998;12: 3752–3763.
23. Clarke PG. Developmental cell death: morphological diversity and multiple mechanisms. Anat Embryol (Berl) 1990;181:195–213.
24. Lockshin RA, Zakeri Z. Programmed cell death and apoptosis: origins of the theory. Nat Rev Mol Cell Biol 2001;2:545–550.
25. Leist M, Jaattela M. Four deaths and a funeral: from caspases to alternative mechanisms. Nat Rev Mol Cell Biol 2001;2:589–598.
26. Kabeya Y, Mizushima N, Ueno T, Yamamoto A, Kirisako T, Noda T, Kominami E, Ohsumi Y, Yoshimori T. LC3, a mammalian homologue of yeast Apg8p, is localized in autophagosome membranes after processing. EMBO J 2000;19:5720–5728.
27. Mizushima N, Yamamoto A, Matsui M, Yoshimori T, Ohsumi Y. In vivo analysis of autophagy in response to nutrient starvation using transgenic mice expressing a fluorescent autophagosome marker. Mol Biol Cell 2004;15:1101–1111.
28. Shintani T, Klionsky DJ. Autophagy in health and disease: a double-edged sword. Science 2004;306:990–995.
29. Kuma A, Hatano M, Matsui M, Yamamoto A, Nakaya H, Yoshimori T, Ohsumi Y, Tokuhisa T, Mizushima N. The role of autophagy during the early neonatal starvation period. Nature 2004;432: 1032–1036.
30. Kitanaka C, Kuchino Y. Caspase-independent programmed cell death with necrotic morphology. Cell Death Differ 1999;6:508–515.
31. Gozuacik D, Kimchi A. Autophagy as a cell death and tumor suppressor mechanism. Oncogene 2004;23:2891–2906.
32. Han JH, Rall L, Rutter WJ. Selective expression of rat pancreatic genes during embryonic development. Proc Natl Acad Sci U S A 1986;83:110–114.
33. Sanders TG, Rutter WJ. The developmental regulation of amylolytic and proteolytic enzymes in the embryonic rat pancreas. J Biol Chem 1974;249:3500–3509.
34. Iwanij V, Jamieson JD. Comparison of secretory protein profiles in developing rat pancreatic rudiments and rat acinar tumor cells. J Cell Biol 1982;95:742–746.
35. Shimizu S, Kanaseki T, Mizushima N, Mizuta T, Arakawa-Kobayashi S, Thompson CB, Tsujimoto Y. Role of Bcl-2 family proteins in a non-apoptotic programmed cell death dependent on autophagy genes. Nat Cell Biol 2004;6:1221–1228.
36. Bockman DE. Morphology of the exocrine pancreas related to pancreatitis. Microsc Res Tech 1997;37:509–519.
37. Taguchi M, Yamaguchi T, Otsuki M. Induction of PDX-1-positive cells in the main duct during regeneration after acute necrotizing pancreatitis in rats. J Pathol 2002;197:638–646.
38. Miettinen PJ, Huotari M, Koivisto T, Ustinov J, Palgi J, Rasilainen S, Lehtonen E, Keski-Oja J, Otonkoski T. Impaired migration and delayed differentiation of pancreatic islet cells in mice lacking EGF-receptors. Development 2000;127:2617–2627.
39. Fukayama M, Hayashi Y, Koike M, Ogawa M, Kosaki G. Immunohistochemical localization of pancreatic secretory trypsin inhibitor in fetal and adult pancreatic and extrapancreatic tissues. J Histochem Cytochem 1986;34:227–235.
40. Nishino I, Fu J, Tanji K, Yamada T, Shimojo S, Koori T, Mora M, Riggs JE, Oh SJ, Koga Y, et al. Primary LAMP-2 deficiency causes X-linked vacuolar cardiomyopathy and myopathy (Danon disease). Nature 2000;406:906–910.
41. Anglade P, Vyas S, Javoy-Agid F, Herrero MT, Michel PP, Marquez J, Mouatt-Prigent A, Ruberg M, Hirsch EC, Agid Y. Apoptosis and autophagy in nigral neurons of patients with Parkinson's disease. Histol Histopathol 1997;12:25–31.1
42. Kegel KB, Kim M, Sapp E, McIntyre C, Castano JG, Aronin N, DiFiglia M. Huntingtin expression stimulates endosomal-lysosomal activity, endosome tubulation, and autophagy. J Neurosci 2000;20:7268–7278.
43. Cataldo AM, Hamilton DJ, Barnett JL, Paskevich PA, Nixon RA. Properties of the endosomal-lysosomal system in the human central nervous system: disturbances mark most neurons in populations at risk to degenerate in Alzheimer's disease. J Neurosci 1996;16:186–199.

Received August 6, 2004. Accepted May 11, 2005.

Address requests for reprints to: Ken-ichi Yamamura, MD, PhD, Institute of Molecular Embryology and Genetics, Kumamoto University, 4-24-1 Kuhonji, Kumamoto 862-0976, Japan. e-mail: yamamura@gpo.kumamoto-u.ac.jp; fax: (81) 96-373-6599.

Supported in part by a Grant-in-Aid on Priority Areas; a Grant-in-Aid from the Ministry of Education, Science, Culture, and Sports of Japan; and a grant from the Osaka Foundation of Promotion of Clinical Immunology.

The authors thank Dr Tamotsu Yoshimori (National Institute of Genetics) for providing the anti-LC3 antibody and Michiyo Nakata for technical assistance.

Available online at www.sciencedirect.com

SCIENCE DIRECT®

Developmental Biology 283 (2005) 357–372

DEVELOPMENTAL BIOLOGY

www.elsevier.com/locate/ydbio

Sonic hedgehog is required for cardiac outflow tract and neural crest cell development

I. Washington Smoak[a,1], N.A. Byrd[b,1], R. Abu-Issa[b], M.M. Goddeeris[c], R. Anderson[c], J. Morris[b], K. Yamamura[d], J. Klingensmith[c], E.N. Meyers[b,c,*,2]

[a]*North Carolina State University, Raleigh, NC 27695, USA*
[b]*Department of Pediatrics, Neonatal-Perinatal Research Institute, Duke University Medical Center, Durham, NC 27710, USA*
[c]*Department of Cell Biology, Duke University Medical Center, Durham, NC 27710, USA*
[d]*Institute of Molecular Embryology and Genetics, Kumamoto University, 4-24-1 Kuhonji, Kumamoto, 862-0976, Japan*

Received for publication 12 November 2004, revised 5 April 2005, accepted 15 April 2005
Available online 4 June 2005

Abstract

The Hedgehog signaling pathway is critical for a significant number of developmental patterning events. In this study, we focus on the defects in pharyngeal arch and cardiovascular patterning present in *Sonic hedgehog* (*Shh*) null mouse embryos. Our data indicate that, in the absence of *Shh*, there is general failure of the pharyngeal arch development leading to cardiac and craniofacial defects. The cardiac phenotype results from arch artery and outflow tract patterning defects, as well as abnormal development of migratory neural crest cells (NCCs). The constellation of cardiovascular defects resembles a severe form of the human birth defect syndrome tetralogy of Fallot with complete pulmonary artery atresia. Previous studies have demonstrated a role for *Shh* in NCC survival and proliferation at later stages of development. Our data suggest that SHH signaling does not act directly on NCCs as a survival factor, but rather acts to restrict the domains that NCCs can populate during early stages (e8.5–10.5) of cardiovascular and craniofacial development.

Keywords: Cardiac; Neural crest; Migration; Pulmonary atresia; Tetralogy of Fallot; Outflow tract; Septation; Anterior heart field; Bmp4; Repulsion

Introduction

Shh is one of three mammalian gene homologues of the extracellular signaling molecule, Hedgehog, first described as a segment polarity gene product in *Drosophila* (Nusslein-Volhard and Wieschaus, 1980). Previous loss-of-function studies in the mouse have demonstrated that *Shh* is required for patterning of several organs such as the nervous system, limbs, lungs, and foregut (Chiang et al., 1996; Litingtung et al., 1998, 2002). Mouse embryos that are homozygous null for *Shh* ($Shh^{-/-}$) are also known to have pharyngeal arch and cardiac defects, but the etiology of these defects has yet to be described in detail (Izraeli et al., 1999; Kim et al., 2001; Meyers and Martin, 1999; Tsukui et al., 1999).

NCCs are ecto-mesenchymal cells that migrate from the junction of the surface ectoderm and neuroectoderm along the dorsal neural tube to populate numerous structures throughout the embryo. Cranial NCCs arise from the forebrain and hindbrain regions to populate craniofacial structures, as well as pharyngeal arches one through three, giving rise to the maxilla, mandible, and other structures of the neck and face (reviewed in Le Douarin and Dupin, 2003; Santagati and Rijli, 2003). Cardiac NCCs populate the third, fourth, and sixth pharyngeal arches, as well as the outflow tract (OT) of the heart and contribute to the smooth muscle of arch arteries in both chick (Kuratani and Kirby, 1992; Nishibatake et al., 1987) and mouse (Jiang et al., 2000). Ablation and genetic studies have shown that NCC production, delamination, directed migration, and survival

* Corresponding author. Duke University Medical Center, PO Box 3179, Durham, NC 27710, USA.
E-mail address: meyer031@mc.duke.edu (E.N. Meyers).
[1] These authors contributed equally to this manuscript.
[2] Current address: University of Wisconsin Medical School, Madison, WI 53706, USA.

0012-1606/$ - see front matter © 2005 Elsevier Inc. All rights reserved.
doi:10.1016/j.ydbio.2005.04.029

are critical for cardiovascular patterning (reviewed in Gitler et al., 2002; Hutson and Kirby, 2003; Maschhoff and Baldwin, 2000). Recent evidence suggests that SHH function is required for NCC survival in chick (Ahlgren and Bronner-Fraser, 1999; Ahlgren et al., 2002) and mouse (Jeong et al., 2004). In this last study, a direct requirement for Hedgehog signals in the development of murine craniofacial NCCs was demonstrated by genetically removing the *Smoothened (Smo)* receptor from migratory NCCs. However, this effect on NCCs appeared after mid-gestation and was not as severe as that demonstrated by functional blocking studies in chick embryos or by the phenotype of $Shh^{-/-}$ mouse embryos, suggesting an additional earlier cell autonomous role for *Shh* in NCC development.

In this study, we sought to characterize the early (e9.5–11.5) cardiovascular and pharyngeal arch development of $Shh^{-/-}$ mouse embryos to better understand how *Shh* expression affects NCC development and these tissues. Our data indicate that *Shh* is required for both NCC and pharyngeal endoderm survival and support *Shh* as a candidate gene defective in patients with tetralogy of Fallot, as well as a possible modifying locus for the 22q11deletion syndromes. Furthermore, mislocalization of NCC derivatives in $Shh^{-/-}$ embryos supports a model where SHH signaling is required for NCC guidance cues.

Materials and methods

Experimental animals

Mouse strains were maintained on an outbred ICR background unless otherwise indicated. This background was chosen because of the multiple transgenes used and the late-term survival with consistent cardiovascular defects. In addition, cardiac looping reversals were absent in $Shh^{-/-}$ embryos on this outbred background, simplifying the analysis of cardiac development at later stages and consistent with previous studies (Izraeli et al., 1999; Tsukui et al., 1999). $Shh^{-/-}$ embryos were generated by intercrossing $Shh^{+/-}$ (Shh^{tm1Chg}) males and females (Chiang et al., 1996). Noon on the day of vaginal plug was designated embryonic (e) day 0.5. More accurate staging was then determined by somite number. Genotyping was by phenotype (late stages) or PCR (early stages) as described (Chiang et al., 1996). All embryos were dissected in either DEPC (diethylpolycarbonate)-treated phosphate-buffered saline (PBS) or PBS with 0.1%Triton X-100 (PBT). Fixation was at 4°C ovemight in 4% paraformaldehyde (PFA) unless otherwise specified.

Cardiovascular system visualization in $Shh^{-/-}$ embryos

$Shh^{+/-}$ males also transgenic for the *Tie2-LacZ* transgene (Tg(TIE2-*lac*Z)182Sato/J), in which *LacZ* is controlled by a *Tie2* endothelial-cell-specific promoter element (Schlaeger et al., 1997), were crossed to $Shh^{+/-}$ females to visualize endothelial structures in $Shh^{-/-}$ embryos. The chest wall/pericardial sac was opened by blunt dissection to better expose the heart and vessels. Embryos were then fixed and washed. β-galactosidase (β-Gal) activity was detected by X-Gal staining. Following staining, embryos were washed, post fixed (4% PFA), and either cleared in 50% glycerol in PBS for whole mount visualization or embedded in paraffin for sectioning using standard procedures (Hogan, 1994).

Generation of $Shh^{-/-}$;P0-Cre;R26R embryos

In order to lineage trace NCCs in $Shh^{-/-}$ embryos, we generated studs that were $Shh^{+/-}$ and transgenic for *P0-Cre* (tg(P0-Cre)1Ky), which expresses the Cre transgene in migratory NCC precursors (Abu-Issa et al., 2002; Yamauchi et al., 1999). These transgenic studs were crossed with $Shh^{+/-}$ female mice that were also transgenic for the CRE reporter, *R26R* (Gt(Rosa)26Sor^{tm1Sor}), which irreversibly expresses *LacZ* in cells that have undergone recombination by the CRE protein (Soriano, 1999). This method allowed us to effectively compare lineage-marked NCCs in $Shh^{-/-}$ and control embryos. *Wnt1-Cre* (Tg(Wnt1-cre)11Rth) males (Danielian et al., 1998) were crossed to R26R females to compare to *P0-Cre* pattern. Embryos were fixed, stained for β-Gal activity, and cleared as described above.

$Ptch1^{LacZ}$

$Ptch1^{LacZ}$, ($Ptch^{tm1Mps}$) with *LacZ* inserted into the *Ptch1* locus, is heterozygous null for *Ptch1* function (Goodrich et al., 1997). Embryos expressing $Ptch1^{LacZ}$ were generated on $Shh^{+/-}$ and $Shh^{-/-}$ backgrounds by generating $Shh^{+/-}$;$Ptch1^{LacZ/+}$ males that were crossed to $Shh^{+/-}$ females.

In situ hybridization

Whole-mount mRNA in situ hybridization was performed as described previously (Neubuser et al., 1997) using digoxygenin-labeled antisense riboprobes constructed from linearized plasmids. Riboprobes were constructed for *Pax1*, *Ap2α*, *CrabP1*, *Bmp4*, *Sox9*, and *Twist*. Embryos were examined at stages indicated within text and figures. All in situ hybridization results were confirmed in at least three $Shh^{-/-}$ mutant embryos and three control embryos that were treated identically.

Whole-mount immunohistochemistry

Immunohistochemistry (IHC) was performed on whole embryos that were fixed and washed in PBS with 0.1%Triton X-100 (PBT). Embryos were placed in blocking solution (BS = 3% bovine serum albumin and 10% sheep or horse serum in PBT) for 1 h then incubated in primary antibody in BS at 4°C overnight. Control embryos were incubated similarly but not exposed to primary antibody.

Embryos were then washed three times for 1 h each in BS diluted 1:5 in PBT, and incubated overnight with secondary antibody in BS. Embryos were washed three times for 1 h each in block diluted 1:5 in PBT and mounted with DABCO or benzyl alcohol:benzyl benzoate as described (Zucker et al., 1999).

Cranial nerves/dorsal root ganglia (DRGs) were visualized with 2H3 antibody (Developmental Studies Hybridoma Bank and developed by T. Jessel and J. Dodd), as described previously (Swiatek and Gridley, 1993) at a primary dilution of 1:100. Cell proliferation was determined by presence of phosphorylated histone H3 (PH3) using anti-phosphorylated rabbit PH3 primary antibody (Upstate Biotechnology) diluted 1:1000.

Cell death analysis

Cell death was demonstrated in whole embryos using Lysotracker™ Red (Molecular Probes) as described previously (Abu-Issa et al., 2002), with the following modifications: sterile lactated ringers was substituted for Tyrode's buffer; 2–4 μM Lysotracker™ was used for 30 min while rotating at 37°C under air; embryos were washed 3 times in lactated ringers and then 4 times in PBS over the course of 30 min at room temperature with gentle inversion. Embryos were then fixed, dehydrated, and cleared as described (Zucker et al., 1999).

TUNEL assays were performed to detect apoptotic cells in paraffin sections. Embryos were fixed in 4% PFA, dehydrated, embedded in paraffin, and sectioned at 6 μm. Sections were deparaffinized, rehydrated, incubated in 2% proteinase K, permeabilized in 0.1% Triton X-100 in 0.1% sodium citrate then incubated with TUNEL reaction mixture (1:20 TdT enzyme per TUNEL Label; Roche) for 60 min at 37°C.

Confocal analysis

Embryos with fluorescent secondary antibodies or Lysotracker were analyzed on a Zeiss LSM 410 or LSM 510 meta Zeiss laser scanning confocal microscope. Z-sectioning series were obtained from using the same settings for controls and mutants, which were then stacked and converted to Quicktime movie images using Zeiss Meta software.

Results

$Shh^{-/-}$ embryos display conotruncal and pharyngeal arch artery defects

Late-term $Shh^{-/-}$ embryos (e16.5–18.5) had consistently (100%) abnormal cardiovascular development which included a single outflow artery arising from the right ventricle instead of the usual two-vessel configuration where the pulmonary trunk arises from the right ventricle and the aorta arises from the left ventricle. The aortic arch was right-sided (normally left-sided) and gave rise to a single midline carotid artery with abnormal subclavian arteries (Figs. 1A,B). While the two ventricles were similar in size, the right was displaced rostrally (pulled up) relative to the left in $Shh^{-/-}$ mutants as previously described (Izraeli et al., 1999; Tsukui et al., 1999). Overall, the mutant hearts were smaller (as were the entire embryos) at this stage of development when compared with controls.

The descending aorta gave rise to abnormal limb arteries; distal to these were collateral pulmonary arteries directed to abnormal lung tissue (Figs. 1C,D). There was no ductus arteriosus. Venous patterning in $Shh^{-/-}$ embryos was notable for abnormal pulmonary vein connections (anomalous pulmonary venous return) as previously reported (data not shown and Tsukui et al., 1999). These findings are consistent with developmental abnormalities observed at earlier stages (see below).

Intracardiac lesions are present in near-term $Shh^{-/-}$ embryos

The atrial septum primum and septum secundum were defective in all mutants examined (n = 5), creating the appearance of a single, common atrium. The two atrioventricular valves were present in most embryos, but the distance separating them was abnormally short (Figs. 1E,F), and in 1 of 5, there appeared to be a single atrioventricular valve. In general, the myocardium was variably thickened in near-term $Shh^{-/-}$ mutants suggesting hypertrophy. No pulmonary valve was detected. Finally, the base of the aorta was shifted rightward with bias to the right ventricle and over-rode a membranous ventricular septal defect (VSD) (Figs. 1G,H). The coronary arteries and epicardium were present and grossly normal.

Aortic arch artery development is abnormal in early $Shh^{-/-}$ embryos

In order to understand the pathogenesis of the defects seen at near term, we next examined the cardiovascular development of $Shh^{-/-}$ embryos between e8.5and e12.5. Aortic arch artery development in mutants also transgenic for the endothelial cell marker *Tie2-LacZ* was compared with littermate controls. The aortic arch arteries arise as condensations of endothelial cell precursors and sequentially develop within the mesenchyme of the pharyngeal arches. In control embryos, progressive development of the first three aortic arch arteries was evident by e9.5 (Fig. 2A). In $Shh^{-/-}$ embryos, the first three aortic arch arteries were hypoplastic, with the first aortic arch artery often single and located at the midline (Fig. 2B). In control embryos, the third, fourth, and forming sixth aortic arch arteries were clearly visible by e10.5 (Fig. 2C), while the fourth and sixth aortic arch arteries in $Shh^{-/-}$ embryos did not appear to develop (Fig. 2D). These data suggest that the right third arch artery rather than the left fourth persists as the aortic

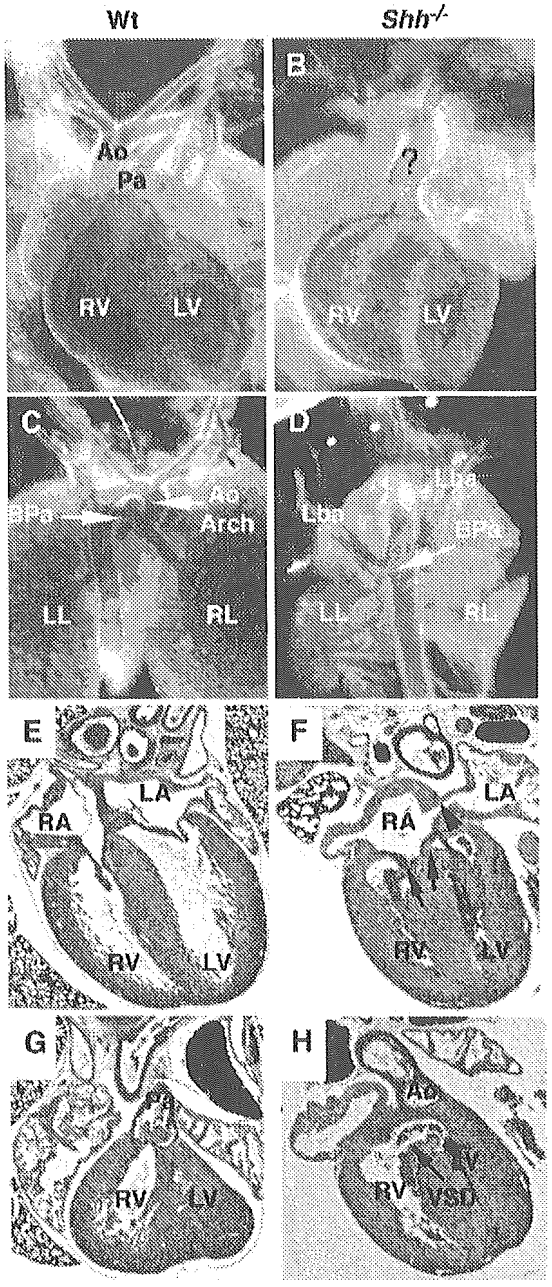

Fig. 1. Comparison of whole-mount *Tie2-LacZ* transgenic (A–D) and histological sections (E–H) of wild type (A,C,E,G) and $Shh^{-/-}$ (B,D,F,H) e16.5 embryos. Ventral view (A,B) demonstrates a single outflow tract (?) rather than aortic (Ao) and pulmonary artery (Pa) as seen in wild-type embryos. Dorsal view (C,D) demonstrates a midline descending Ao with branch pulmonary arteries (BPa) arising from the descending aorta distal to abnormal limb arteries (Lba) rather than off the main pulmonary artery as in control (D vs. C arrow). Sectioning of the hearts demonstrates an absent atrial septum (black arrowhead), abnormal atrioventricular valves (arrows), and thickened ventricular muscle (F) compared with controls (E). The Ao outflow was malpositioned (H) between the right and left ventricles (RV and LV) overriding a ventricular septal defect (VSD). LL—left lung, RL—right lung, RA—right atrium, LA—left atrium.

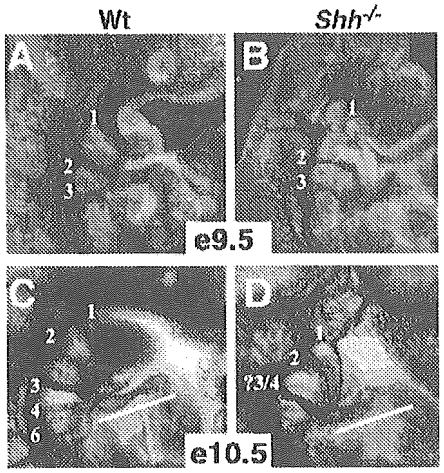

Fig. 2. Arch artery development was abnormal in *Tie2-LacZ* transgenic $Shh^{-/-}$ embryos (B,D) compared to controls (A,C). As early as e9.5, $Shh^{-/-}$ embryos have hypoplastic arches (particular 1st arch) and abnormal vascular endothelial cell pattern (B vs. A). By e10.5, only the right 3rd arch artery is well formed in $Shh^{-/-}$ mutants with no apparent 4th or 6th arch artery development (D vs. C).

arch in $Shh^{-/-}$ embryos. In addition, the pharyngeal space and the aortic sac in $Shh^{-/-}$ embryos was much smaller and narrower than in controls. This reduction in overall size appeared to be secondary to the reduced width and size of the pharyngeal arches and pharyngeal region.

Conotruncal development is abnormal in early $Shh^{-/-}$ embryos

We next compared conotruncal development between $Shh^{-/-}$;*Tie2-LacZ* and control embryos. Surprisingly, OT lengthening was impaired, and development of the pulmonary portion was deficient prior to the arrival of migratory NCCs. At e9.0 (23 somites), $Shh^{-/-}$ hearts already demonstrated subtly smaller OT and right ventricle relative to the inflow and left ventricle (data not shown). At e10.5 (35 somites), when NCCs first enter the OT, there was already a marked difference in OT and right ventricle length between mutants and controls (Figs. 3A–D, compare white bars). The shortening of the OT appears to result in the right ventricle being "pulled" toward the pharyngeal region relative to the left ventricle. By e11.5 (43 somites—when NCCs have populated the OT), the combined length of the OT and right ventricle were markedly smaller, and the left portion of the OT lacked an endothelial channel (Figs. 3E–H). In addition, there appeared to be less rostral/caudal compression of the endothelial tract (Figs. 3G vs. H, arrowheads). By e12.0–12.5, the single outflow tract in $Shh^{-/-}$ embryos was continuous with the right third aortic arch artery with a hypoplastic left 3rd arch artery, while the pulmonary channel was completely absent (Figs. 3I–L, black arrows). No consistent defects were noted in the myocardium of e9.5–12.5 $Shh^{-/-}$ embryos, suggesting that any myocardial abnormalities seen near-term are secondary to pressure/flow

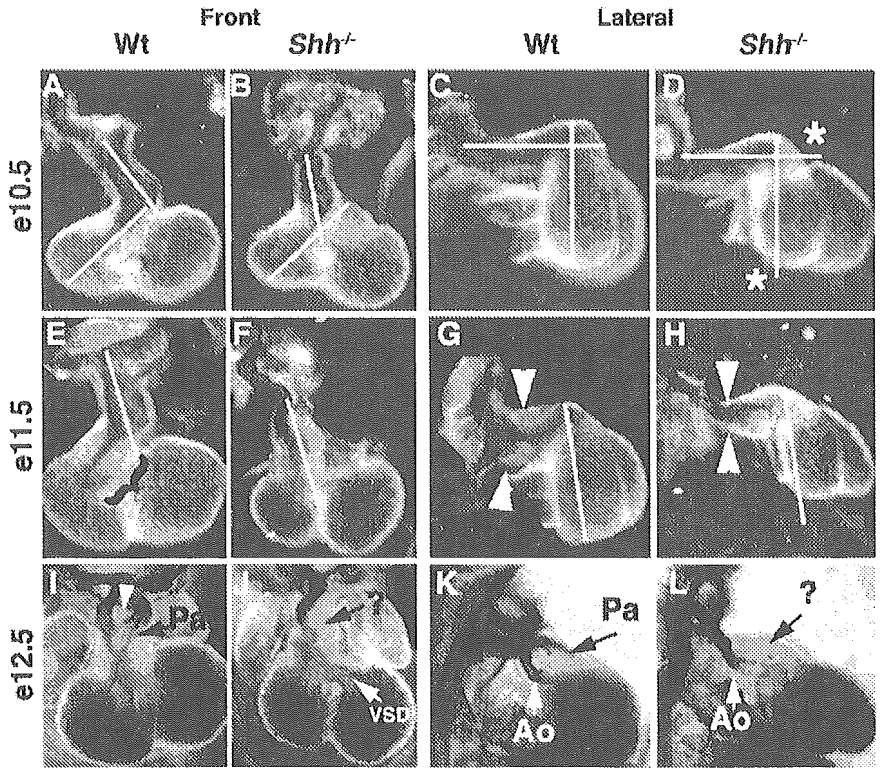

Fig. 3. Outflow tract development was abnormal in $Shh^{-/-}$ embryos. Using *Tie2-LacZ*, outflow tract and ventricular development were visualized after X-Gal staining in embryos at e10.5 (37 somites: A–D), e11.5 (43 somites: E–H), and e12.5 (I–L). Wt and *Shh* mutants as marked. White bar is identical in length in adjacent figures. At 37 somites, both the distal truncus (B vs. A) and conus/right ventricle (D vs. C) of the developing outflow tract were smaller. This difference persisted and became more apparent particularly in the conus/right ventricular portion of the outflow tract at 43 somites (H vs. G). In addition, the truncus was thin and the endothelial channel less flattened by presumptive NCCs (G vs. H, white arrowheads). By 43 somites, the pulmonary endothelial channel was not forming, and a VSD was present between ventricles (I–L), demonstrating development of pulmonary artery atresia.

changes associated with defects in the outflow tract and pharyngeal arch arteries or a later function of *Shh*.

$Shh^{-/-}$ embryos have hypoplastic pharyngeal arches and loss of arch derivatives

One of the most striking defects observed by gross examination of $Shh^{-/-}$ embryos at early stages was abnormal development of the pharyngeal arches. Hypoplasia of the first pharyngeal arch could be identified in $Shh^{-/-}$ embryos as early as e9.0. The first pharyngeal arches were abnormally fused in the midline, and the distance between the remaining left and right pharyngeal arches was significantly reduced. To evaluate for defects of pharyngeal arch-derived structures, we examined sections and bone preparations of $Shh^{-/-}$ embryos at e16.5–18.5.

The first through third pharyngeal arches and pouches contribute to a number of structures such as the face/neck bones, external/internal ear, as well as several glands in the neck (thymus, thyroid, and parathyroid glands). Virtually all of the structures derived from the first through sixth pharyngeal arches/pouches were abnormal or absent in $Shh^{-/-}$ embryos (data not shown). Craniofacial structures essentially consisted of only a nasal and otic capsule. Notably, there was a small thymus present in mutants, consistent with other reports (Fagman et al., 2004; Moore-Scott and Manley, 2005).

Most or all of the defects described in $Shh^{-/-}$ embryos are consistent with loss of the pharyngeal arch and pouch derivatives of which NCCs are a major component. In addition, NCCs are required for arch artery and OT development. Given previous evidence that *Shh* signaling can affect NCC development, we next examined the specification, migration, and fate of NCCs in $Shh^{-/-}$ embryos.

Neural crest cells are specified though migrate abnormally in $Shh^{-/-}$ embryos

NCCs are specified and migrate in $Shh^{-/-}$ embryos as determined by *CrabP1* and *Ap2α*, two markers expressed in migrating NCCs (Dencker et al., 1990; Mitchell et al., 1991). We found that, while both *CrabP1* and *Ap2α* were expressed at grossly normal levels, the pattern of expression was abnormal in *Shh* mutants (Figs. 4A–D). *CrabP1* was not expressed in the first arch, and there was fusion of the post-otic tracts of neural crest (third and fourth arch) into one broad stream (Fig. 4A vs. B). Similarly, *Ap2α*, which is normally expressed in the dorsal neural tube and DRGs and

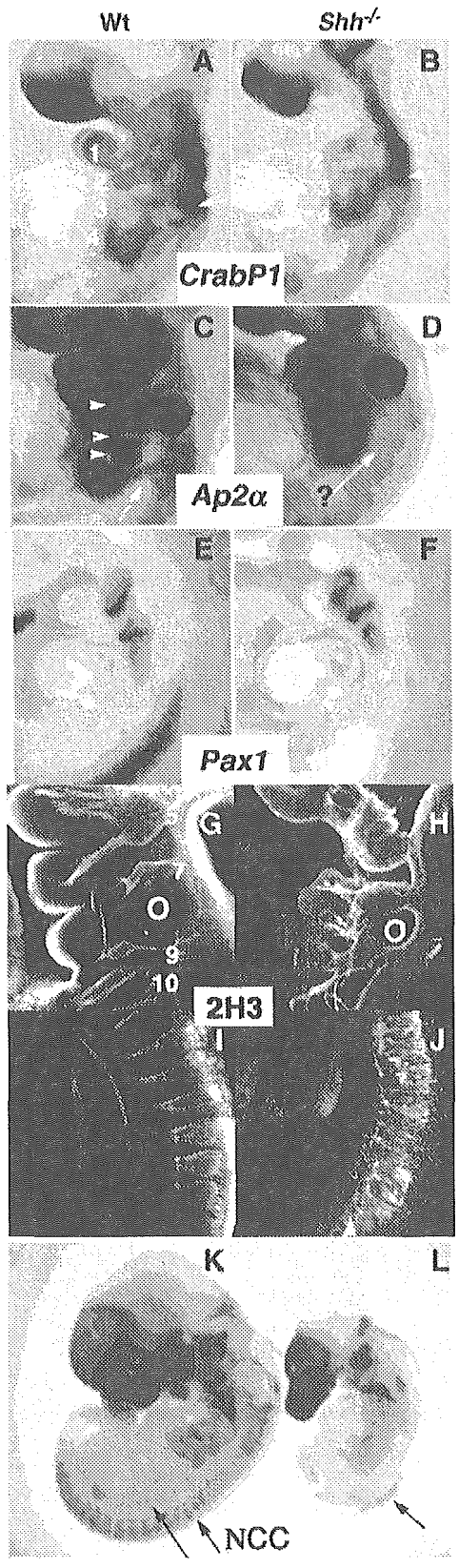

along distinct paths into the arches, was more diffuse and misexpressed in tissue including the ventral neural tube of e10.5 *Shh*$^{-/-}$ embryos (Fig. 4C vs. D). This altered expression pattern could be the result of abnormal arch segmentation independent of NCC expression. However, examination of the endodermally expressed transcription factor *Pax1* demonstrated that the arches were well defined and separated in *Shh*$^{-/-}$ embryos (Figs. 4E,F). At e11.5, a general reduction in the number of cells positive for *Ap2α* and *CrabP1* was seen in *Shh*$^{-/-}$ mutants (data not shown).

The pattern of *Ap2α* and *CrabP1* suggested that NCCs were migrating along abnormal pathways. To further study this phenomenon, we examined the expression of the neurofilament specific antibody, 2H3, which marks the NCC-derived cranial nerves and DRGs (Figs. 4G–J). Strikingly, the cranial nerves and DRGs were abnormally fused and more broadly distributed, respectively, consistent with the previous *Ap2α* and *CrabP1* mRNA analysis.

Shh$^{-/-}$ *embryos have a reduced population of NCC derivatives*

To study the fate of NCCs in greater detail, we generated *Shh*$^{-/-}$ embryos that were also transgenic for *P0-Cre* (expressed by migrating NCCs) and the Cre reporter R26R. This strategy allowed us to effectively compare lineage marked NCCs in *Shh*$^{-/-}$ embryos and controls. At e10.5, a marked decrease in β-Gal positive cells in the pharyngeal arches of *Shh*$^{-/-}$ embryos (data not shown) suggested that loss of arch tissue in the mutants resulted from a reduced NCC population. In addition, there is a general reduction in the expression of *LacZ* in the DRGs. By e11.5, this general loss of NCCs is even more striking (Figs. 4K,L). NCCs did enter the cardiac OT but appeared to be decreased in number and in an abnormal pattern in *Shh*$^{-/-}$ embryos. In control hearts, NCCs entered the outflow tract in two discrete prongs, whereas NCCs entering the outflow tract in *Shh*$^{-/-}$ embryos were distributed along the walls and not in distinct prongs of cells (see Fig. 8). The general reduction in NCC numbers

Fig. 4. Expression of NCC markers demonstrate induction and migration but an abnormal pattern in *Shh* mutants. At e9.5, *CrabP1* expression was absent in the 1st arch, and the distinct streams of NCCs in arches 3–4 were fused into one (B vs. A and arrow). At e10.5, *Ap2α* expression was more widespread than normal with no distinction in the arches (arrowheads), loss of specific NCC tracts, and diffuse signal in areas of the trunk (arrow) in *Shh* mutants (D vs. C). Expression of the endodermal specific marker *Pax1* demonstrated that the arches were well segmented in *Shh* mutants like controls, although expression was missing from the developing somites (E–F). Examination of cranial nerves (CN) and DRGs utilizing the neurofilament antibody 2H3 (see Materials and methods) demonstrated fusion of CN 7, 9, and 10 in *Shh* mutants (G vs. H) as well as abnormal DRGs and sympathetic chain ganglia with indistinct borders (I vs. J). Lineage trace of NCCs (K–L) utilizing *P0-Cre* and the Cre reporter R26R (see Materials and methods) demonstrated a reduced number of NCC derivatives with marked reduced population within the craniofacial region and arches as well as abnormal or absent DRGs by e11.5 (arrows). O—otocyst.

after induction suggests that NCCs fail to proliferate and/or survive in *Shh*$^{-/-}$ embryos. Together, these results indicate that NCCs are specified but localize abnormally and are markedly reduced in number as early as e10.5.

NCCs proliferate normally in Shh$^{-/-}$ *embryos*

Given the reduced number, we next examined cell proliferation of NCCs using an anti-phospho-histone H3 antibody that labels cells in metaphase. Confocal laser microscopy optical sections of e9.5 and e10.5 embryos demonstrated no significant difference in proliferation within the arches of *Shh*$^{-/-}$ embryos (n = 3) compared to control littermates (data not shown). However, we cannot rule out that subtle differences in proliferation, or changes in proliferation occurring at earlier stages, contribute to the decreased NCCs seen in these mutants.

Shh$^{-/-}$ *embryos exhibit increased cell death within the arches and pharyngeal endoderm*

We examined cell death in whole mount *Shh*$^{-/-}$ embryos by using both TUNEL (data not shown) and the fluorophore Lysotracker Red which indicates necrotic or dying cells (Zucker et al., 1999). Strikingly, there were marked areas of increased cell death in the arches of *Shh*$^{-/-}$ embryos. Confocal laser optical sections demonstrated that at e9.0 there were small amounts of cell death in the forebrain and at the mid-hindbrain boundary of control embryos (Figs. 5A–C). In contrast, *Shh*$^{-/-}$ mutants had a marked increase in cell death in forebrain, midbrain, around the developing eye, and cells adjacent to the neural tube (suggestive of migratory NCCs) (Figs. 5E–G). These zones of cell death are consistent with the defects previously described in these mutants, including forebrain and mid-hindbrain defects (Chiang et al., 1996; Moore-Scott and Manley, 2005). At e10.0, there were several small areas of cell death in wild type embryos, including a moderate population migrating from the mid-hindbrain region into the first pharyngeal arch (data not shown), a smaller population immediately around the developing otocyst, and a population at the proximal junction of the first and second pharyngeal arches (Figs. 5H–J). In *Shh*$^{-/-}$ embryos, there was a dramatic increase in cell death in cells of the developing arches, as well as cell death present in the developing pharyngeal endoderm. Optical sections revealed that virtually all of the first and second arch mesenchymal cells were dying, particularly distal arch cells (Figs. 5K–M). At e10.5, the endoderm and presumptive NCCs entering the outflow tract were also dying, unlike controls (Figs. 5O,P).

Ptch1 expression suggests a role for Shh in NCC localization

In order to understand how loss of *Shh* affects pharyngeal arch, NCCs, and cardiovascular development,

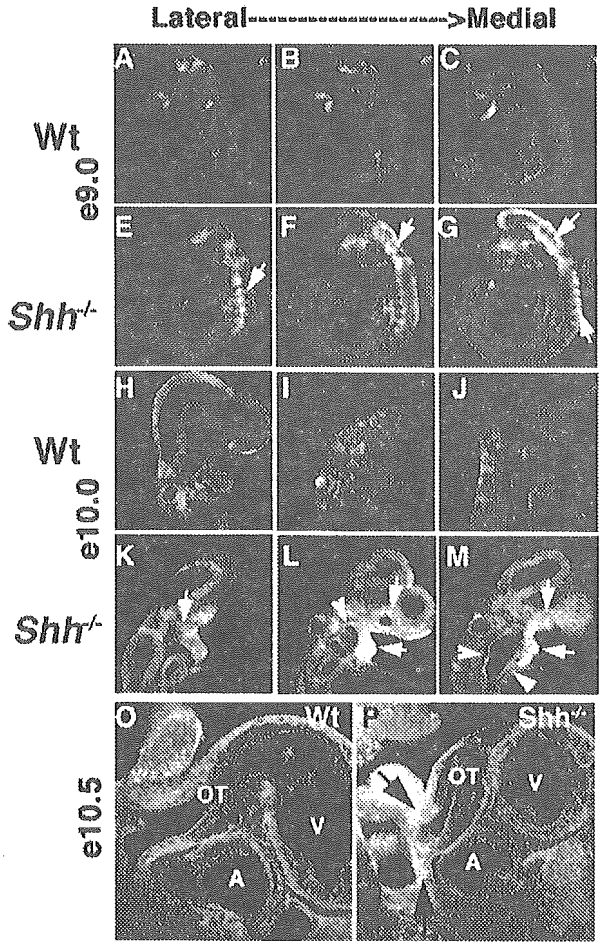

Fig. 5. Confocal laser optical sections of whole-mount Lysotracker-treated embryos demonstrated excessive cell death in *Shh* mutants (E–G, K–M, P) when compared with controls (A–C, K–M, O). At e9.0 (A–G), lateral to medial sagittal sections revealed increased cell death in the neural tube and cells adjacent to the neural tube of a *Shh* mutant (arrows in panels E–G vs. A–C). At e10.0–10.5 (H–P), there was increased cell death in cells of the pharyngeal arches as well as around the cyclopic eye and forebrain (arrows) and pharyngeal endoderm (arrowheads) of *Shh* mutants (K–M v. H–J). Higher magnification demonstrated the marked death of cells approaching the outflow tract (OT) contiguous with cushions and endothelial channel, as well as throughout the endoderm (arrows in panel P vs. O). A—atrium, V—Ventricle.

we next examined the expression of *Shh* and its receptor *Ptch1*, which reflects the extent of SHH signaling (and other Hedgehog family members) from the source of expression (Goodrich et al., 1997; Zhang et al., 2001). As previously reported, *Shh* mRNA is extensively expressed within the pharyngeal arch endoderm (Jeong et al., 2004). However, no expression in mesenchyme of the arches, around the developing arch arteries or within the OT, was detected (Figs. 6A,B and data not shown). *Ptch1* mRNA and *Ptch1*^{LacZ} expression were both examined and were similar. The expression of both *Ptch1* mRNA and *Ptch1*^{LacZ} is much more extensive than *Shh* expression itself. Within the developing pharyngeal arches, expression

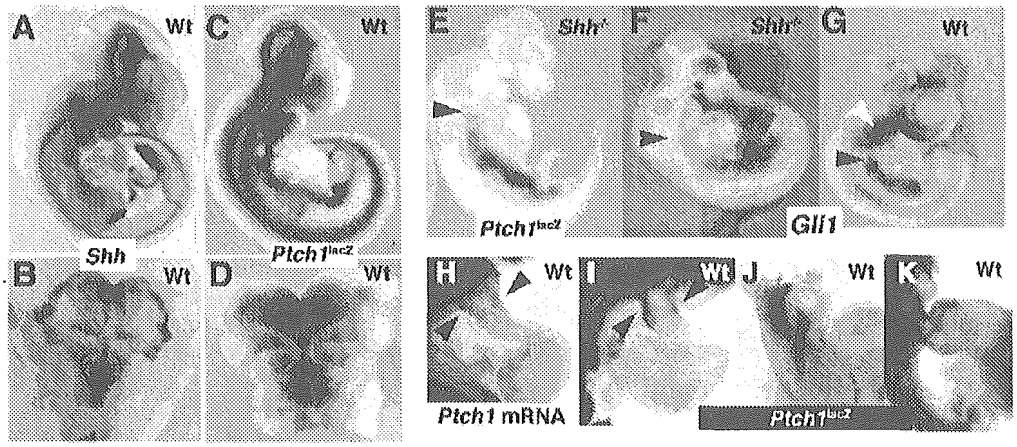

Fig. 6. Comparison of *Shh* mRNA expression to ß-Gal activity from *Ptch1*^{LacZ} demonstrated broader expression of *Ptch1*^{LacZ} reflecting diffusion of Hedgehog pathway signals (A vs. C). Within the ventral pharyngeal region, *Shh* (B) was present and restricted to the endoderm, while *Ptch1*^{LacZ} (D) was in both endoderm and adjacent mesenchyme with high expression in the developing thyroid. The *Ptch1*^{LacZ} (E) and *Gli1* mRNA (F) domains in *Shh*$^{-/-}$ embryos were restricted to the developing gut at e10.5 when compared to controls (C and G), indicating that no other family member was actively signaling in the pharyngeal region or neural tube at these stages. *Ptch1* mRNA (H) and to a greater extent *Ptch1*^{LacZ} (I) were expressed into the OT at e10.5 of wild-type embryos (arrowheads). *Ptch1*^{LacZ} was expressed in two prongs that spiral into the OT (J) and continued to be expressed in the septating OT (K).

was detected in the pharyngeal endoderm and extended into the mesenchyme of the arches (Figs. 6C,D and Jeong et al., 2004). To determine to what extent *Ptch1*^{LacZ} pharyngeal expression reflects SHH signaling and not that of other Hedgehog family members, we examined the expression of *Ptch1*^{LacZ} in *Shh*$^{-/-}$ embryos. Between e9.5–11.5, significant β-Gal activity was detected only in the developing gut and not within the arches or the OT (Fig. 6E vs. C). To confirm that signaling through other members, perhaps through *Ptch2* receptor, was not occurring within the pharyngeal endoderm, we also examined expression of *Gli1*, another direct downstream target of Hedgehog signaling. Similar to *Ptch1*^{LacZ}, expression of *Gli1* was seen only in the developing gut of *Shh*$^{-/-}$ embryos at this stage (Fig. 6F vs. G), indicating that pharyngeal arch expression of *Ptch1* is mediated by SHH at these stages.

One surprising area of *Ptch1* expression was within the developing OT itself (Fig. 6H), which was more apparent with the *LacZ* allele than mRNA (Fig. 6I). This expression started as early as e9.5 and persisted through septation of the OT (e12.5). Initially, two lines of expression extended into the distal OT (Fig. 6J) and later surrounded the developing distal aorta and pulmonary trunk (Fig. 6K). *Ptch1*^{LacZ} expression was noted in the outflow of *Shh*$^{-/-}$ embryos after e11.5, suggesting that other Hedgehog signaling family members may be active in heart development at later stages (data not shown).

Given the observed NCC deficits and the pattern of *Ptch1*^{LacZ} expression, we next asked whether SHH acts directly on NCCs by determining if NCCs express the *Ptch1* receptor. To address this issue, we compared somite stage-matched *Ptch1*^{LacZ} and *P0-Cre;R26R* embryos stained for ß-Gal activity. We found that, between e9.5–11.5, *Ptch1*^{LacZ} expression was essentially absent from NCCs and instead complimentary to lineage traced NCCs with little apparent overlap.

At e10.5, *Ptch1* expression was seen in mesenchyme medially, whereas NCCs migrating into the pharyngeal arches populate more lateral regions (Figs. 7A–D vs. E–H). As cells enter the OT, *Ptch1* expression encompasses the ventral pharynx, including the septum forming from the dorsal aortic sac, while NCCs are adjacent (Figs. 7A,B vs. E,F). Around the arch arteries, *Ptch1* expression is restricted to the medial region, while *P0-Cre*-marked NCCs are localized laterally (Fig. 7C vs. G). Through e11.5, this complimentary pattern of *Ptch1* expression relative to NCCs remained consistent. Whereas pharyngeal tissue more dorsal–medial remains *Ptch1* positive, NCCs remain more lateral in discrete domains (Figs. 7I–L vs. M–P). These relatively mutually exclusive domains persist into the OT as well (Fig. 7K vs. O). Sectioning of e10.5 outflow tracts revealed that *Ptch1* expression was present in the myocardial wall of the OT adjacent to areas where endothelial cells abut the myocardial wall to the exclusion of NCCs (Figs. 7Q–S vs. T–V). This pattern suggests that one possible role for *Shh* signaling at this stage may be to restrict the domains that NCCs populate. This pattern was also present in other areas of NCC development such as the developing stomach, where NCC-derived enteric neurons form (Figs. 7W,X). To confirm that our *P0-Cre* transgene was faithfully marking NCC, we also examined *Wnt1-Cre* lineage traced NCC at e11.5. While there are differences in the pattern generated by *P0-Cre* versus *Wnt1-Cre*, a similar complimentary pattern to *Ptch1*^{LacZ} was obtained (Fig. 7M vs. M′). These data indicate that *Ptch1* is not expressed by the majority of NCCs, and, therefore, SHH does not signal directly to a significant number of NCCs at these stages.

Our examination of OT development suggested that the defects in pulmonary artery development primarily occurred

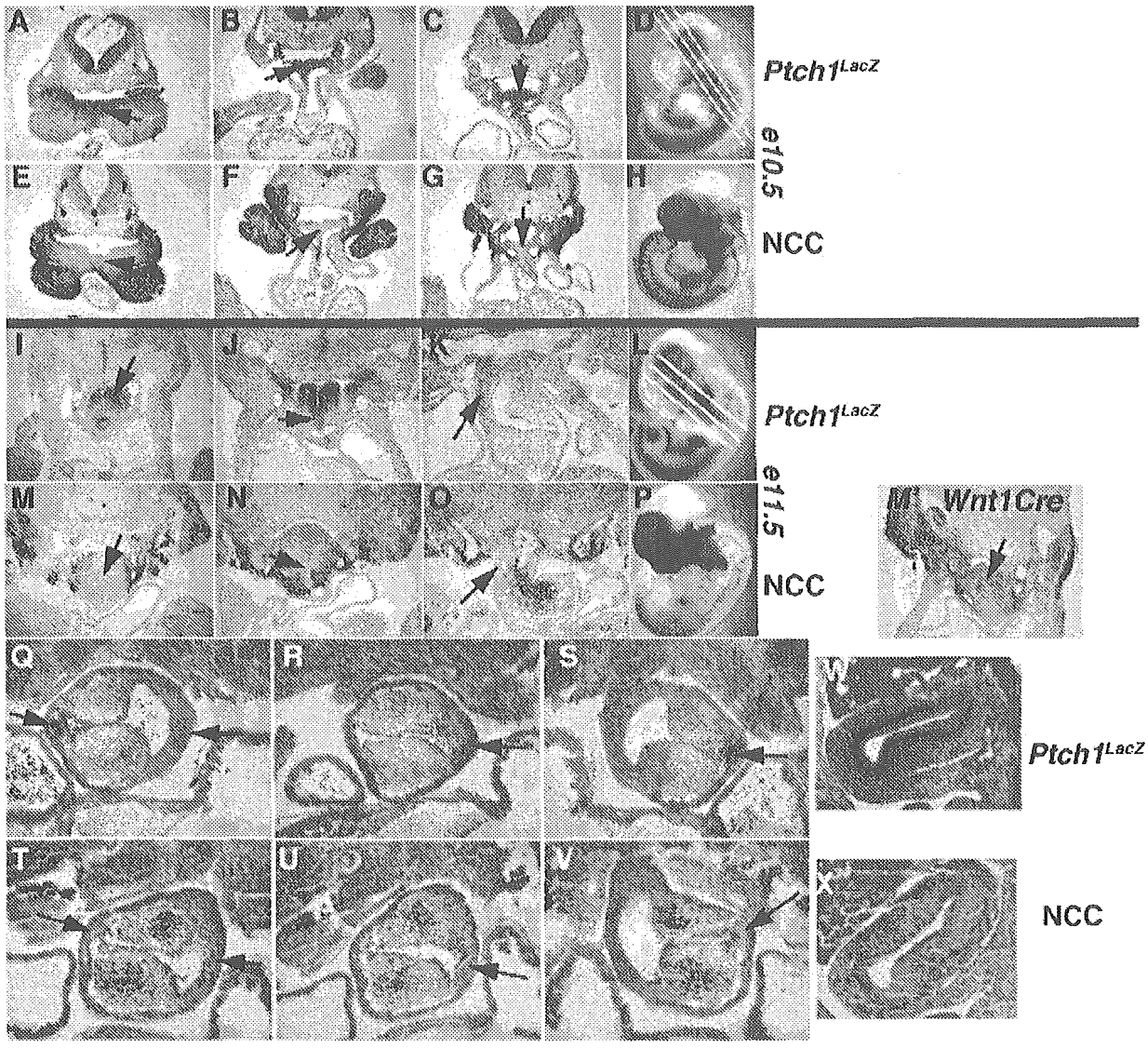

Fig. 7. *Ptch1*^{LacZ} expression was complementary to NCC derivatives between e10.5 and e11.5. Somite-matched *Ptch1*^{LacZ} (A–D, I–L, Q–S) were compared with *P0-Cre:R26R* (E–H, M–P, T–V) embryos. Approximate pharyngeal frontal sections (white bars D) showed NCC to be excluded from *Ptch1*^{LacZ} domains at both e10.5 (A–D vs. E–H) and e11.5 (I–L vs. M–P). Arrows in complementary sections (i.e., A vs. E) demonstrate where *Ptch1* expression was present and NCCs were not. Sections through e10.5 OT localized *Ptch1*^{LacZ} to the areas where the endothelial channel abuts the myocardium to the exclusion of NCCs (arrows Q–S vs. T–V). The relationship of NCCs to *Ptch1*^{LacZ} persisted in other areas of NCC migration such as the gut where NCC-derived enteric neurons populate (W vs. X). *P0-Cre:R26R* (M) results were comparable to *Wnt1-Cre:R26R* (M').

between e10.5 and e11.5 (Fig. 3). Therefore, we reasoned that perhaps the pulmonary artery was absent because the pulmonary endothelial channel was being obstructed by abnormal NCC localization in *Shh*$^{-/-}$ mutants. We therefore examined stage-matched e10.5 hearts from *Shh*$^{-/-}$ and control embryos to compare NCC, *Ptch1*^{LacZ}, and *Tie-LacZ* expression patterns (Fig. 8).

As previously demonstrated in section, the expression of *Ptch1*^{LacZ} is complimentary to NCC localization and apparently adjacent to where endothelial cells are closest to the myocardial wall (Figs. 8A–F). Comparison of the NCC to the endothelial patterning again demonstrates that there is a significant reduction in the NCCs entering as the OT of *Shh*$^{-/-}$ embryos. The OT is narrower, and there is no cranial–caudal compression of the endothelial channel by NCCs as seen in controls (Fig. 8I vs. J). However, some NCCs do enter the outflow tract but appear as a bolus of cells in the area of the forming pulmonary artery (Figs. 8G,K vs. H,L, and Figs. 3J,N). Interestingly, this area appears to correspond to where *Ptch1*^{LacZ} is expressed and where the pulmonary artery connects to the forming sixth arch arteries (Figs. 8F,K,L). We confirmed this finding by lineage tracing NCCs in *Shh*$^{-/-}$ embryos. Examination of the outflow tract reveals a diffuse pattern of reduced NCC

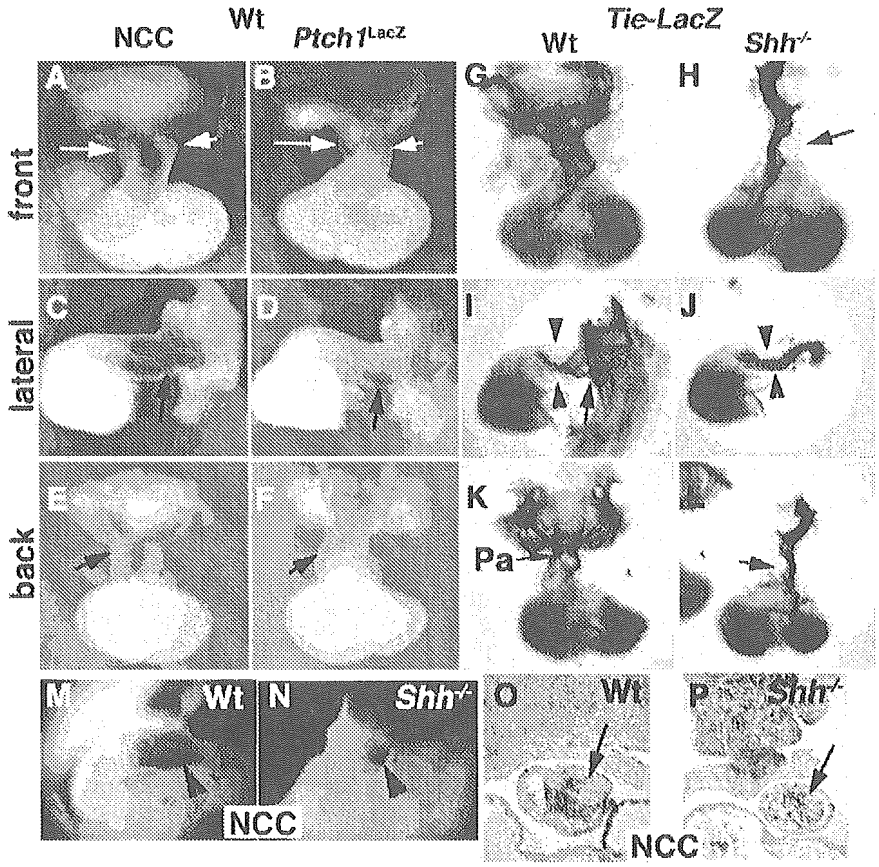

Fig. 8. Analysis of NCC, *Ptch1*^{LacZ}, and endothelial cell markers during OT septation in removed hearts at e11.5. Hearts are viewed as marked. Whole-mount wild-type NCC pattern compared to *Ptch1*^{LacZ} confirmed the complementary pattern (A,C,E vs. B,D,F). At the same stage, *Tie2-LacZ* staining demonstrated abnormal endothelial compression by NCCs in *Shh* mutants (G,I,K vs. H,J,L). A bolus of cells was present in the OT of mutants (arrow H,L) that corresponded with the location of the developing pulmonary artery (Pa in K) as well as the location of *Ptch1*^{LacZ} expression (arrows in D,F) and absent NCCs (arrows C, E). NCC tracing in *Shh*$^{-/-}$ embryos confirmed decreased and abnormal distribution of cells in whole-mount e12.5 OT (M vs. N) and sectioned e11.5 embryos (O vs. P arrow).

localization (Figs. 8M,N). Sectioning of e11.5 outflow tracts revealed a more diffuse representation of NCCs during septation when compared to controls (Fig. 8O vs. P). These data indicate that less NCCs populate the OT and that they are mislocalized in *Shh*$^{-/-}$ embryos.

NCC derivatives are mislocalized in Shh$^{-/-}$ *embryos*

To further pursue our observation that NCCs are mislocalized, we examined other non-cardiovascular structures in *Shh*$^{-/-}$ embryos. *Ap2α* mRNA expression in the developing neural tube of *Shh* mutants was localized throughout the neural tube but appeared absent laterally in whole mount at e11.5. However, upon closer examination, expression was seen ventral to the neural tube (Figs. 9A–C). In addition, *Shh*$^{-/-}$*;P0-Cre;R26R* embryos clearly demonstrated that DRGs are fused at the ventral midline, with neuronal tracts abnormally crossing the midline (Figs. 9E,F) where *Ptch1*^{LacZ} is normally expressed (Fig. 9D). In addition to crossing the midline, DRGs were also fused in the rostral–caudal axis (Figs. 9H,I). Examination of *Ptch1*^{LacZ} showed lateral segmented expression domains (Fig. 9G), suggesting that *Shh* signaling is critical for separating the NCC-derived DRGs in this axis, as well as left and right sides. Examination of the pharyngeal arches also demonstrated ectopic localization of NCCs to the dorsal pharyngeal region and other areas (Figs. 9J–L, 8O). Interestingly, examination of the stomach and gut demonstrated relatively normal localization of neural crest derived enteric neurons consistent with the continued expression of *Ptch1*^{LacZ} (reflecting Hedgehog signaling other than SHH within the gut). Furthermore, in the area of the developing abdomen, the DRG development was more segmental, suggesting perhaps some rescue from other Hedgehog signals localized within the gut (Fig. 4L and data not shown).

How are NCCs indirectly affected by SHH signaling?

We detected loss of NCCs both at the time of delamination as well as during migration. This loss must be primarily indirect as *Ptch1* does not appear to be expressed